# Dynamics of Sensory Integration of Olfactory and Mechanical Stimuli Within the Response Patterns of Moth Antennal Lobe Neurons

Harrison Tuckman $^*$  and Jungmin Kim $^\dagger$  and Aaditya Rangan $^\ddagger$  and Hong Lei $^\S$  and Mainak Patel $^\P$ 

#### Abstract

Odors emanating from a biologically relevant source are rapidly embedded within a windy, turbuluent medium that folds and spins filaments into fragmented strands of varying sizes. Environmental odor plumes therefore exhibit complex spatiotemporal dynamics, and rarely yield an easily discernible concentration gradient marking an unambiguous trail to an odor source. Thus, sensory integration of chemical input, encoding odor identity or concentration, and mechanosensory input, encoding wind speed, is a critical task that animals face in resolving the complex dynamics of odor plumes and tracking an odor source. In insects, who employ olfactory navigation as their primary means of foraging for food and finding mates, the antennal lobe (AL) is the first brain structure that processes sensory odor information. Although the importance of chemosensory and mechanosensory integration is widely recognized, the AL itself has traditionally been viewed purely from the perspective of odor encoding, with little attention given to its role as a bimodal integrator. In this work, we seek to explore the AL as a model for studying sensory integration – it boasts well-understood architecture, well-studied olfactory responses, and easily measurable cells. Using a moth model, we present experimental data that clearly demonstrates that AL neurons respond, in dynamically distinct ways, to both chemosensory and mechanosensory input; mechanosensory responses are transient and temporally precise, while olfactory responses are long-lasting but lack temporal precision. We further develop a computational model of the AL, show that our model captures odor response dynamics reported in the literature, and examine the dynamics of our model with the inclusion of mechanosensory input; we then use our model to pinpoint dynamical mechanisms underlying the bimodal AL responses revealed in our experimental work. Finally, we propose a novel hypothesis about the role of mechanosensory input in sculpting AL dynamics and the implications for biological odor tracking.

**Keywords:** neuronal network models; antennal lobe dynamics; computational neuroscience; olfactory modeling

# 1 Introduction

Integration of chemosensory input (encoding odor identity and concentration) and mechanosensory input (encoding wind velocity) is critical for olfactory navigation and the ability of insects to home in on and locate an odor source [48]. One particularly crucial task for an insect is the ability to track an odor source mid-flight. This ability is critical for finding food, but poses a monumental challenge: turbulent wind eddies produce complex patterns of odor strands of different sizes and concentrations intermixed with clear media, obfuscating the odor source and rarely yielding an easily discernible 'concentration gradient' to follow [65, 9, 53]. To successfully track an odor, an insect must simultaneously classify odor identity and rapidly resolve the spatio-temporal dynamics of the odor plume, all while maintaining balance and bearing during flight.

<sup>\*</sup>Department of Mathematics, William & Mary; Williamsburg, VA, 23187; USA

<sup>&</sup>lt;sup>†</sup>Current address: Department of Pharmacology, University of Colorado Denver, Aurora, CO, 80045; USA

<sup>&</sup>lt;sup>‡</sup>Courant Institute of Mathematical Sciences, New York University, NY, NY 10012; USA

<sup>§</sup>School of Life Sciences, Arizona State University, Tempe, AZ, 85281; USA

<sup>&</sup>lt;sup>¶</sup>Department of Mathematics, William & Mary; Williamsburg, VA, 23187; USA

Corresponding Author: mjpatel@wm.edu

Evidence strongly suggests that the ability of insects to track odors mid-flight relies on the integration of mechanical with chemical input, and, accordingly, chemosensory and mechanosensory bimodality is indeed widespread within the central nervous system of insects. In terms of sensory organs, while Johnston's organ and Böhm's bristles on the antenna are well known to detect wind velocity and guide flight maneuvers [57, 29, 61], there are also less studied bimodal sensilla [29, 61]. For example, a subtype of trichoid sensilla on the antenna of the male hawkmoth [39] and sensilla chaetica on the honeybee antenna [71] exhibit chemoand mechano-sensory bimodality. A wide range of animals have been shown to be adept at intelligently sampling environmental odor plumes to home in on an odor source [3, 56, 58, 64]; moths, in particular, employ a strategy in which they surge upwind upon encountering odor strands and cast across wind when losing contact with odors [66]. This suggests that chemosensory and mechanosensory input may augment and corroborate each other, consistent with the close link between odor plume structure and air turbulence; the apparent convergence on this strategy across many species reveals the importance of sensory integration in tracking odor sources.

The antennal lobe (AL), consisting of excitatory projection neurons (PNs) and inhibitory local neurons (LNs) organized into cellular clusters called glomeruli, is the first brain area to substantially process odor information arriving from olfactory receptor neurons (ORNs) in the sensory periphery. While the AL has been traditionally investigated within the domain of odor (and  $CO_2$ ) detection, there exist some data in moths and other insects suggesting that AL neurons are actually bimodal [20, 33, 18]; recently, a study in tadpoles [8] and a couple of studies in mice [28, 4] have shown that olfactory bulb glomeruli are responsive to mechanosensory input (in the absence of odor) arising from air pressure. Unfortunately, such data are sparse, and little attention has been given to developing models of sensory integration within the AL models of AL function and dynamics have thus far focused on the AL from a purely chemosensory perspective. Hence, the network mechanisms and dynamics underlying sensory integration within the AL, and the biological significance of the interplay of olfactory and mechanical input within the AL, remain poorly understood, despite the fact that sensory integration is an important aspect of odor tracking. The AL, however, is an otherwise ideal system for the study of bimodality – specifically, AL architecture is well understood, AL odor response dynamics are well-studied, and AL neurons are easy to measure individually and in aggregate. Additionally, the anatomy and physiolology of the AL is analogous to that of the olfactory bulb (OB) in vertebrates [23], and hence may provide insight into chemo- and mechano-sensory integration in a broad range of species.

In this work, we seek to explore the interaction between chemosensory and mechanosensory input within the AL, and propose possible network mechanisms underlying observed PN response patterns. We begin by presenting some preliminary data within the moth showing that PNs within the AL respond to both olfactory and mechanosensory signals, and that these two sources of input may influence AL dynamics in starkly disparate ways. These data suggest that strong mechanosensory input may enhance the amplitude and temporal precision of AL odor responses – i.e., that high speed nonscented air (mechanosensory input alone) elicits a transient, temporally precise burst of activity in PNs, while an odor delivered at low wind speed (low mechanosensory input) tends to induce a more prolonged response in PNs, and odor delivered at high wind speed (high mechanosensory input) tends to combine features of both mechanosensory and olfactory response patterns in isolation.

To examine the network dynamics underlying our early experimental observations, we construct a large-scale biophysical model of the moth AL, with physiologically reasonable components and parameters, consisting of PNs and LNs organized into glomeruli. Furthermore, we simulate both olfactory and mechanosensory input to the model, under the reasonable assumption that mechanosensory input is less focal in the glomeruli it targets than olfactory input. We first probe the responses of our model network to odor input alone, and we not only show that our model exhibits the triphasic odor responses observed experimentally in moth PNs [11, 69, 12, 13, 16], but we also dissect model dynamics to provide plausible mechanistic explanations for how such response patterns arise. We then explore model responses to mechanosensory input alone, and show that the transient, temporally precise nature of responses to mechanosensory signals arises naturally from model dynamics as a consequence of pervasive slow inhibition activated via excitation of the global LN network. Finally, we show that model dynamics are capable of capturing empirically observed response patterns to olfactory and mechanosensory input in combination, and we examine the implications of bimodality for odor discrimination and tracking.

Section 2 describes our experimental and theoretical results (with experimental results prior to section

2.1 and modeling results in sections 2.1-2.4), section 3 provides our discussion, while section 4.1 and 4.2 describe our experimental and computational methods, respectively.

# 2 Results

In the male sphinx moth Manduca sexta, the cell bodies of sex pheromone-sensitive uniglomerular AL PNs are located within the medial cluster, a convenient target for identifying PNs (figure 1A); dye injection into glomerular neuropil often results in partial staining at the soma. Data from such PN recordings, in response to scented and non-scented air puffs at various air flow speeds, are shown in figure 1. We recorded from a total of 9 PNs, most of which (7 out of 9) showed a clear increase in spike rate in response to non-scented air puffs. One representative example is shown in figure 1. This PN displayed clear responses to mechanical stimulation alone (figure 1D), with a stronger response to air puffs infused with pheromone (which provides both chemical and mechanical stimulation) (figure 1E). Furthermore, within our recorded PN population, increasing the puffing speed of non-scented air puffs from 0.5 liter/min (low speed) to 1 liter/min (high speed) increased the intensity of the response of the PN population, as shown in figure 1B,D. Other published work within the AL has reported similar phenomena [20, 18].

We further parse the dependence of the PN response on air speed from the data displayed in figure 1. The sample PN did not respond to non-scented air puffs at low speed (figure 1B), but displayed a clear, long-lasting response to pheromone-infused air puffs at low speed (figure 1C); the correlation coefficient of these two response patterns (based on peri-stimulus time histograms) is rather low (r=-0.19). However, at high air-puffing speed, the PN exhibited a rather robust bursting response to non-scented puffs (figure 1D), but showed a clear and substantial increase in response intensity to pheromone-infused air puffs at the same speed (figure 1E); interestingly, these two response patterns are remarkably similar (r=0.67).

In figure 2, we summarize and quantify response features of each of our recorded PNs. We define a PN as being responsive to mechanosensory input if the peak response to high speed air puffs, based on its peri-stimulus time histogram, exceeded 1.5X its background activity – based on this metric, we find that 7/9 of our recorded PNs respond to mechanosensory input, and we include only these 7 PNs in figure 2. Figure 2A shows the peak firing rate, while figure 2B shows the temporal duration, of the responses of each of the 7 PNs to high-speed air puffs, phereomone at low puffing speed, and pheromone at high puffing speed.

In most cases, odor-laden high speed air puffs (which impart both a strong olfactory and mechanical signal) induce larger peak responses than nonscented high speed air puffs (which convey only a strong mechanosensory signal). Odor-laden low speed air puffs (which impart a strong olfactory signal with little mechanosensory content) yield varying peak responses, presumably due to variability in the number of input ORNs or in the affinity of input ORNs for the employed odor. However, it is worth noting that in most cases the response to odor-laden high speed air puffs is larger than that to odor-laden low speed air puffs; since responses to high speed nonscented air puffs are larger than responses to low speed nonscented air puffs (as described above), this suggests that, in these cases, a strong mechanosensory signal augments the reponse induced by the olfactory signal alone (figure 2A).

Figure 2B shows that, in most cases, the response to odor-laden low speed air puffs exhibits a longer temporal length than the response to nonscented high speed air puffs, suggesting the relatively transient nature of PN responses to isolated mechanosensory input versus isolated olfactory input. Interestingly, there is some diversity in the the temporal duration of PN responses to high speed odor-laden air puffs; in some cases, the duration of the response to high speed odor-laden air puffs is similar to the (generally short) response duration for high speed nonscented air puffs, while in other cases, the duration of the response to high speed odor-laden air puffs is similar to, or even longer than, the (generally lengthier) response duration for low speed odor-laden air puffs.

Thus, the data indicate that most PNs (7/9) respond robustly and diversely to strong mechanosensory input (i.e., high wind speed), even in the absence of an olfactory signal. Moreover, mechanical and chemical input appear to trigger distinct response patterns in PNs – strong mechanosensory input alone elicits a transient, temporally precise burst of spikes lasting a few hundred ms, while olfactory input with low air flow (at low wind speed, mechanical input is reduced) yields a more prolonged, sustained spiking response that is hence less temporally precise. The observed transiency of the response to purely mechanosensory

input is consistent with recordings shown in other published work (e.g., see figure 10A of [33]). When the two modalities are combined (i.e., odor delivered at high wind speed), strong mechanosensory input often augments the intensity of the olfactory response, while response length can be short and transient (as with mechanosensory stimulation alone) or prolonged (as with olfactory input in isolation). In the case of a prolonged response, both the isolated mechanosensory input and isolated olfactory input response patterns can contribute to PN dynamics, with the PN response to high speed odor-laden air puffs exhibiting a large, transient, temporally precise burst of spikes followed by a lower-intensity sustained spiking response (as exhibited by the sample PN shown in figure 1E).

Finally, it is tantalizing that there is a high correlation between a PN's response pattern to strong mechanosensory input alone and its response pattern to strong mechanosensory input plus olfactory input. This suggests that, in natural environments, strong mechanosensory input may serve to mold and shape the dynamic, correlational structure of PN responses across the AL network. This possibility will be elaborated upon further within the *Discussion* section.

## 2.1 Model Construction

In order to examine the mechanisms underlying AL responses to olfactory or mechanosensory input, as well as the juxtaposition of the two, we construct a realistic, large-scale, spiking-network model of the moth AL; the model consists of six glomeruli, with 10 PNs and 6 LNs per glomerulus [25, 35, 27, 22, 49, 10, 26]. Individual PNs and LNs are governed by integrate-and-fire spiking dynamics, with random but fixed network connectivity – LNs synapse onto other LNs within the same glomerulus and onto PNs both within and across glomeruli, while PNs synapse only onto PNs and LNs within the same glomerulus [59, 42]. LNs are GABAergic and inhibit other neurons through fast GABA<sub>A</sub> receptors, and LNs also deliver a slow inhibitory current to PNs, acting over  $\sim$ 500-1000 ms time scales, via slower metabotropic GABA receptors. PNs within the model are cholinergic and act synaptically through fast nicotinic acetylcholine receptors; PNs are also equipped with an intrinsic calcium-dependent potassium (SK) current that activates following several PN spikes and serves to curtail further spiking [51, 50].

We simulate both chemosensory and mechanosensory input to the model, both in isolation and in conjunction. In accordance with the well-established combinatorial odor code employed by olfactory receptor neurons (ORNs) [31, 67, 68, 47, 1, 70, 54], an odor (in the absence of significant mechanosensory input) is simulated by delivering an excitatory stimulus current to all cells within a subset of model glomeruli (half of model glomeruli are designated to receive stimulus current); different odors are simulated by varying the composition of the glomerular subset receiving stimulus current.

Mechanosensory input, on the other hand, is modeled by sending stimulus current to cells within all network glomeruli. Thus, in our model we make the assumption that mechanosensory input is less local, and at least somewhat more widespread, in its glomerular targets than olfactory input arising from a typical odorant. While it is well known that chemosensory input from a typical odorant tends to target a highly localized glomerular subset, due to the combinatorial nature of the ORN odor code and the relatively strict one-to-one mapping of ORN types onto AL glomeruli, the extent or number of glomeruli targeted by mechanosensory input is less well-known. Our data suggest the possibility that mechanosensory responses within the moth AL may be relatively widespread across glomeruli, but we cannot definitively derive this conclusion from our data. Another suggestive piece of evidence, though, is that responses to nonscented air puffs can be observed in recordings from ORNs – e.g., see [55], figure 4 of [60], and figure 1 of [38]. Hence, ORNs themselves may be the source of mechanosensory input to the AL; if this is the case, then it may be reasonable to hypothesize that more ORNs respond to mechanosensory input than chemosensory input from a typical odorant, since chemoselectivity arises from the fact that each ORN tends to express a single type of olfactory receptor (among many), while mechanoselectivity does not exist – any ORN that can sense mechanical stimuli will provide mechanosensory input. Thus, while our modeling assumption of mechanosensory input targeting a broader swath of glomeruli than olfactory input has not yet been experimentally verified, we believe that it is a reasonable one. Moreover, we note that the modeling results described in this manuscript (namely, the transiency of the response to mechanosensory signals) can also be obtained by sending mechanosensory input to only 3 or 4 (rather than all 6) glomeruli – all that is required to obtain transient responses to mechanosensory input in isolation is that the mechanosensory signal is weak and 'enough' of the global LN network is activated by the signal (i.e., a weak mechanosensory signal

- near the strength employed in the present model – elicits weakly active PNs, and if this signal is sent to 3 or 4 glomeruli, then the global LN network is sufficiently activated by the signal to suppress these weakly excited PNs after an initial burst).

We employ two paradigms to simulate both modalities in conjunction (i.e., an odor delivered within the context of strong mechanosensory input due to high wind speed): (i) Additive Paradigm – the stimulus current due to mechanosensory input and odor input are simply added together to construct the high wind speed odor stimulus; (ii) Normalized Paradigm – the stimulus current due to mechanosensory input and odor input are both halved in amplitude then added together. Paradigm (i) may be more akin to physiological reality, since PN responses from our data (figure 1) are suggestive of the possibility that the mechanosensory response and the odor response of a PN augment each other to obtain the response to an olfactory signal delivered at high wind speed. Paradigm (ii) allows analysis of network dynamics when net excitation to the AL is kept approximately constant in the three cases of odor input alone, mechanosensory input alone, and odor+mechanosensory input, permitting a more distilled comparison of the dynamical effects of the two modalities in isolation and in conjunction. Figure 3 shows a schematic of the model network. Model details can be found in the Methods.

## 2.2 Model Dynamics To Olfactory Input In Isolation

Taking advantage of modeling power, we begin by probing model responses to olfactory input alone (i.e., without simulating mechanosensory input), modeled as strong, focal stimulus current delivered to a subset of AL glomeruli (glomeruli 1,2, and 3). We verify that model responses to olfactory input alone recapitulate the salient features of experimentally observed moth AL odor dynamics, and we further dissect the dynamical mechanisms underlying model behavior. Experimentally, during prolonged odor presentation PNs within activated glomeruli tend to exhibit a characteristic triphasic response; the first phase ( $I_1$ ) occurs at odor onset and consists of a brief membrane potential hyperpolarization that lasts  $\sim 50$  ms, after which rapid depolarization accompanied by spiking ensues for the duration of the stimulus (phase II), while odor offset triggers the third phase ( $I_2$ , also called the AHP phase) of hyperpolarization followed by a slow recovery back to background over  $\sim 1$  sec [11, 69, 12, 13, 16].

Figure 4A depicts a raster plot of AL spiking activity in response to odor input - PNs within stimulated glomeruli tend to exhibit robust responses to the odorant, while PNs within nonstimulated glomeruli are suppressed, due to pervasive network-wide LN inhibition induced by the stimulus [59, 42]. Figure 4A further shows that PNs within activated glomeruli exhibit the characteristic triphasic odor response observed experimentally. Phase I (the  $I_1$  phase) occurs due to the stimulus current inducing LNs to reach threshold prior to PNs; hence, odor onset yields an initial burst of synchronized LN spikes within activated glomeruli, leading to compounded fast inhibition from LNs briefly hyperpolarizing and silencing glomerular PNs. Following the initial burst of LN spikes, LN activity desynchronizes and diminishes slightly (due to LN $\rightarrow$ LN fast synaptic inhibition), allowing PN depolarization to commence and phase II PN spiking to ensue. This is consistent with experimental evidence showing that direct GABA application mimics an  $I_1$ -type response in PNs and that the GABA antagonist bicuculline (BIC) eliminates the  $I_1$  phase of odor-evoked PN activity [69, 12, 16, 17]; indeed, blockade of fast GABAergic synapses within our model eliminates the phase I hyperpolarization of PNs following odor onset (figure 6A).

However, while experiments indicate that the  $I_1$  response seems driven by  $GABA_A$  receptors, the mechanisms underlying the phase II response and the AHP (or  $I_2$ ) phase are empirically less well-understood. During the phase II response, PN spike patterns can vary broadly across PNs; within active glomeruli, some PNs fire spikes in sporadic or irregular bursts, while others fire more continuously at moderate ( $\sim 50$  Hz) firing rates, with a range of response patterns intermediate between the extremes of bursting and continuous firing. Moreover, the phase II dynamics exhibited by a PN shows no spatial dependency – in fact, a significant amount of intraglomerular variability has been observed during stimulation [43, 15].

Our model exhibits similar variability in phase II PN response patterns (figure 4A), with examples of a continuously firing PN and a bursting PN shown in figures 4B and 4C, respectively. Within our model, the phase II behavior of a PN is primarily determined by the strength of its SK current – the strength of the SK current of each PN within our model is randomly drawn from a Gaussian distribution, leading to inherent variability in SK current strength across PNs and hence the diversity in PN phase II response patterns. Figure 5A shows spike rasters when the SK current is removed from our network (left) or fixed

at a high value for all PNs (right), suggesting that a lack of SK currents tends to yield continuously firing PNs, while potent SK currents tend to produce burst-like PN behavior. This is further corroborated by measuring the phase II behavior of a single, fixed PN as the strength of its SK current is varied – figure 5B shows that the phase II response pattern of a PN undergoes a clear, progressive, and gradual transition from continuous firing behavior to sporadic bursting behavior as SK strength is increased. Indeed, within the normal network (with randomly drawn SK strengths), there is a substantial correlation between the degree of burst-like behavior and SK current strength across PNs (figure 5C). Thus, this result represents an experimentally testable prediction of the model – the model predicts that, in the moth AL, the strength of the SK current varies across PNs, and that a PN's SK current strength determines the nature of its phase II response pattern.

Within our model, the AHP (or  $I_2$ ) phase of lengthy hyperpolarization following prolonged odor presentation emerges as a dynamical consequence of slow inhibition from LNs to PNs. During phase II spiking in the midst of prolonged odor presentation, the slow inhibitory current activates and exerts a damping effect on PN spiking, but the potent odor-induced current impinging upon stimulated glomeruli is still able to elicit substantial PN spiking responses. Upon odor offset, however, the odor-induced current rapidly dissipates, while slow inhibition from LNs to PNs decays over a longer 1-2 second time scale, allowing the gradually dwindling slow inhibitory current to suppress PN activity for  $\sim$ 1 second following odor offset. Indeed, severing slow inhibitory synapses within the model virtually eliminates the AHP phase of PN odor dynamics, and PNs return to background activity levels immediately following odor offset (figure 6B).

# 2.3 Model Dynamics With Mechanosensory Input

We now examine the behavior of our model with the inclusion of strong mechanosensory input, simulated as a one second current pulse delivered to all glomeruli, though weakened in comparison to an odor-induced current pulse to a stimulated glomerulus (an odor alone, as in the previous section, is simulated as a stronger one second current pulse delivered to only three glomeruli). Thus, we construct four stimulus scenarios: (i) odor only, with no mechanosensory input, which simulates odor delivered at low wind speed; (ii) mechanosensory input only, which simulates a nonscented, high speed air puff; (iii) additive paradigm of high wind speed odor delivery, simulated by simple summation of the current pulses in the odor-only and mechanosensory-only scenarios; (iv) normalized paradigm of high wind speed odor delivery, simulated by halving then summing the current pulses in the odor-only and mechanosensory-only scenarios. The additive paradigm is likely more representative of the physiological reality of moth AL dynamics in response to high wind speed odor presentation (our moth data in figure 1 suggest that PN responses to high wind speed odor stimuli may be augmented relative to responses to either mechanosensory input alone or odor input alone). However, the normalized paradigm maintains similar net excitation to the AL as in the odoronly and mechanosensory-only scenarios, allowing direct comparison of scenarios (i), (ii), and (iv); this permits distillation of the dynamical effects of odor input and mechanosensory input alone, and the two in conjunction, without the potential confound posed by variation in the net integrated excitation impinging

Figure 7 shows spike rasters of the AL model (left) and the trial-averaged firing rate of a sample PN in the network (right) in response to the four stimulus scenarios. In the odor-only scenario, PNs within stimulated glomeruli exhibit substantial spiking throughout the duration of the stimulus, with only a modest differential elevation in firing rate occurring specifically at stimulus onset (figure 7A). In the mechanosensory-only scenario, however, PNs throughout the entire AL respond with an intense spike burst at stimulus onset, but within a few hundred milliseconds are rapidly suppressed to background or lower than background activity levels, and subsequently remain in this suppressed state for the duration of the stimulus (figure 7B). Thus, model behavior is consistent with the experimental data shown in figures 1 and 2 – purely mechanosensory input yields transient, temporally precise PN responses followed rapidly by suppression, while olfactory input without a strong mechanical signal (i.e., odor delivered at low wind speed) yields a more prolonged and sustained spiking response. Furthermore, we note that the brief and transient nature of the response to purely mechanosensory input is a feature that *automatically* emerges from model dynamics, despite the prolonged nature of the current pulse simulating mechanosensory input.

The response of our model AL to strong mechanosensory input in conjunction with odor input (figure 7C,D) combines features of the responses to the two modalities in isolation. All AL PNs respond with a

sharp burst of spikes at stimulus onset (with PNs in glomeruli receiving odor input displaying considerably higher-frequency spiking within the burst), while following the burst, for the remainder of the stimulus duration, PNs within glomeruli receiving odor input continue firing at rates substantially elevated above background (though considerably diminished in comparison to the prior spike burst) and PNs within glomeruli not receiving odor input are strongly suppressed below background. The responses of our model PNs to odor and mechanosensory input in conjunction (odor delivered at high wind speed) therefore capture the salient features of the behavior of the experimentally recorded PN shown in figure 1 under similar stimulus conditions – a response with a high-intensity transient, temporally precise component followed by a lower-intensity longer-lasting component. The data in figure 2 suggest that a few of our exmperimentally recorded PNs exhibit somewhat different response dynamics than our model PNs, in that their responses to strong mechanosensory input in conjunction with odor input are relatively brief and are more akin to responses to purely mechanosensory input; while we do not incorporate the behavior of such PNs within our model, we note that such behavior can be captured within our model in a relatively simple manner, and merely requires adjusting the relative strengths of olfactory versus mechanosensory input to individual PNs.

This leads to a natural query: how do model dynamics give rise to such qualitatively discordant behavior in response to the two modalities? In other words, why are responses to odor input long-lasting while those to strong mechanosensory input are transient and brief, despite the temporally prolonged nature of both stimuli? The answer lies within the dynamics of the inhibitory current (particularly slow inhibition) from LNs to PNs, coupled with the globally extensive nature of the glomeruli-spanning LN network (and the relatively weak nature of mechanosensory input, compared to odor-induced input). Figure 8A shows the AL response to strong mechanosensory input alone in the absence of slow inhibition, fast inhibition, or the SK current, and suggests that the lack of slow inhibition produces the most profound effect on eliminating the transient nature of responses to mechanosensory input; this is further quantified in figure 8C (left), which shows that PN firing rates during the latter half of a one second mechanosensory input pulse tend to be higher in the absence of slow inhibition versus in the absence of other network components. Since LN neurites traverse glomeruli to synapse onto PNs thoughout the AL, the mechanosensory signal, which activates all glomeruli, yields global activation of the LN network, and hence globally pooled slow inhibition is delivered to all network PNs; the potency of this pooled slow inhibitory current, coupled with the mechanosensory signal to each PN being relatively small in amplitude, ensures that, after a few hundred ms (once the slow inhibition activates and rises in strength) network PNs are hyperpolarized and silenced. In the case of an odor input alone, on the other hand, only a subset of glomeruli receive stimulus current, and activation of this LN subset does not generate enough pooled slow inhibition to overcome PN responses to the relatively large-amplitude stimulus current, leading to long-lasting PN responses (though PNs within nonstimulated glomeruli are indeed suppressed by the slow inhibitory current).

It should be noted that figure 8C (left) indicates that fast inhibition plays a substantial role in producing the transient nature of responses to mechanosensory input alone as well, and hence that, within the model, fast inhibition augments the slow inhibitory current to produce response suppression during the latter half of stimulus presentation (i.e., response suppression is due to fast inhibition + slow inhibition). In our simulations, however, we find that strengthening slow inhibition (in the absence of fast inhibition) is capable of producing transient responses to isolated mechanosensory input, while strengthening fast inhibition (in the absence of slow inhibition) is not capable of producing the same transient dynamics. If fast inhibition is strengthened sufficiently without slow inhibition, then the entire response – during the entire period of stimulus presentation – is suppressed (since fast inhibition activates rapidly over time scales of a few ms, it is incapable of having a differential effect on the first 500 ms versus the second 500 ms of a stimulus response); on the other hand, if slow inhibition is strengthened sufficiently in the absence of fast inhibition, then there exists a range of values for the strength of slow inhibition in which the latter half of the stimulus response is suppressed while the former half of the stimulus response is not, due to the slow rise time of the slow inhibitory current (data not shown). In this work, we therefore focus on the slow inhibitory current as the primary element driving the transiency of response dynamics to mechanosensory input in isolation.

This suggests that if the potency of slow inhibition were sufficiently enhanced, then PN responses to odor input alone would also begin to display a more transient quality (since, presumably, slow inhibition from even a subset of network LNs would then be sufficient to silence PNs). This is exemplified in figure 8B, which shows the spike response of a sample glomerulus to a one second pulse of mechanosensory input alone

(left) or odor input alone (right) for varying levels of pervasive slow inhibition within the network. For very low levels of slow inhibition, responses to both mechanosensory input alone and odor input alone are long lasting, while for very high levels of slow inhibition responses to both stimulus modalities are transient, brief, and rapidly curtailed by the rising slow inhibitory current. For mid-range levels of slow inhibition within the network, however, PN responses to mechanosensory input are transient and brief (global LN activation is sufficient to suppress PN responses), while PN responses to odor input are long-lasting (local LN activation does not produce enough network-wide slow inhibition to suppress PN responses). This observation is quantified in the center and right panels of figure 8C, which show that slow inhibition levels within a moderate, mid-level range, during the latter half of a one second stimulus pulse, yield strong suppression of PN responses in the case of mechanosensory input alone but substantial PN spiking in the case of odor input alone.

# 2.4 Odor Discrimination Dynamics Within The Model

Experimental studies show that simultaneous presentation of multiple odors can actually have a damping effect on responses within the moth AL, often resulting in less intense network-wide PN activation than in the case of single-odor presentation [45, 62, 72]. Our model exhibits behavior consistent with these empirical observations – simultaneous presentation of two odors that activate sufficiently disparate sets of glomeruli triggers network-wide inhibition that is stronger than the enhancement in excitatory ORN input to the network resulting from simulating two odors (rather than a single odor), producing a net suppressive effect on model dynamics (figure 9A). This is due to the diffuse, glomeruli-spanning LN network [59, 42]; simultaneous presentation of two odors, provided the odors activate minimally overlapping glomerular subsets, activates a broad swath of this LN network (in comparison to a single odor), resulting in a substantial increase in the barrage of globally pervasive slow (and fast) inhibitory inputs impinging upon PNs across glomeruli that more than offsets the greater stimulus-induced excitation.

We further assess the ability of PN activity within our model to classify different odors. Since a single odor within our model is represented by the identity of the three (out of six) glomeruli that receive odor-induced stimulus current, this implies that our model is capable of simulating a suite of 20 distinct odorants. We employ a simple linear classification scheme to test the ability of PN activity within the model to discriminate among the panel of twenty odorants – each odorant is represented by a template, given by the trial-averaged vector of PN firing rates in response to presentation of the odor (100 trials per odor), and each trial is designated as 'correctly classified' by the network if the distance between the vector of PN firing rates corresponding to that trial to the various odor templates is minimized for the correct odor template (see *Methods* for details). We note that this scheme merely represents a simple way to ascertain the separation between odor representations in our model AL, and may not fully capture the complexity of the manner in which downstream mushroom body neurons decode AL activity in vivo.

Figure 9B (left) shows the correct classification rate of the network, computed in 10 ms windows, over a one second odor pulse; in general, the odor alone (with no mechanosensory input) stimulus scenario exhibits the greatest accuracy in odor classification in comparison to the stimulus scenarios which include mechanosensory input (the additive or normalized sensory integration scenarios). This matches intuitive expectations – the mechanosensory signal is nonspecific and independent of odor identity; thus, the mechanical signal cannot impart any information about odor identity, and is more likely to confound and imbue an element of ambiguity into existing odor identity information. Accordingly, odor classification is reduced most strikingly in the normalized sensory integration stimulus scenario, since in this scenario the olfactory signal is diminished in strength, along with the presence of the potentially confounding mechanosensory signal.

The most informative comparison in terms of odor discrimination, however, is between the odor-only and additive sensory integration scenarios, since the odor signal is fixed across both these cases, and hence the effect of mechanosensory input on odor classification can be directly assessed. Interestingly, figure 9B (left) indicates that while the odor-only scenario yields more accurate odor classification during the initial few hundred ms of the odor response, the additive sensory integration scenario actually yields slightly higher classification rates during the subsequent few hundred ms of the odor response (with the two scenarios yielding comparable performance after  $\sim 500$  ms). The reason for this can be ascertained by comparing spike rasters of odor-stimulated glomeruli in the two scenarios (figure 7A versus figure 7C); note that, in

glomeruli receiving olfactory input, the initial burst of PN spikes at odor onset in the additive sensory integration case outlasts the initial burst in the odor-only case by a few hundred ms, which presumably enhances the separation between distinct odor templates in the 60 dimensional PN phase space for the additive sensory integration scenario in comparison to the odor-only scenario (beginning a few hundred ms after odor onset and ending  $\sim$ 500 ms after odor onset). Thus, odor discrimination is better in the additive sensory integration case versus the odor-only case during this brief temporal window.

This feature of odor classification dynamics is an emergent consequence of the slow inhibitory current from LNs to PNs. In the odor-only scenario, odor-stimulated glomeruli receive less net ORN input than in the additive sensory integration scenario, since in the latter scenario odor-stimulated glomeruli receive the odor-induced signal (as in the former scenario) plus additional excitation from the mechanosensory signal. This implies that stronger slow inhibition is required to substantially dampen PN spiking in odorstimulated glomeruli in the additive sensory integration scenario than in the odor-only scenario; however, since the activation time scale of slow inhibition is similar in the two scenarios, substantial dampening of PN responses during the initial stimulus-induced high-frequency spike burst takes a greater length of time in the additive sensory integration scenario than in the odor-only scenario. Thus, due to the temporal dynamics of the activation of the slow inhibitory current, there exists a brief time window, beginning a few hundred ms after odor onset and ending ~500 ms after odor onset, during which PNs within odorstimulated glomeruli spike at a substantially higher rate in the additive sensory integration scenario than in the odor-only scenario, and odor classification is hence more accurate in the former scenario during this brief epoch. Indeed, as evident from figure 9B (right), blockade of slow inhibitory synapses within the network leads to removal of this brief epoch, yielding odor classification rates in the odor-only scenario that surpass those in the additive sensory integration scenario for the entire first  $\sim 500$  ms of stimulus presentation. Overall, since the first few hundred ms of an odor response are likely the most behaviorally relevant for an insect, it is reasonable to suggest that odor classification is, for practical purposes, diminished with the addition of mechanosensory input (even with the inclusion of slow inibition).

# 3 Discussion

In this work, we present experimental evidence showing that PNs within the moth AL respond not only to ambient olfactory stimuli, but also to mechanosensory signals arising from high-speed air flow across the antennae, supporting the idea that the AL is a structure that integrates input from multiple sensory modalities (rather than simply responding to olfactory input). Additionally, our experimental work suggests that olfactory and mechanosensory signals induce starkly different response dynamics within the AL - olfactory input tends to induce long-lasting PN responses that lack temporal precision, while in constrast mechanosensory input leads to brief, temporally precise PN responses. We then develop a biophysically detailed model of the moth AL that captures many salient features of moth AL odor responses reported in the literature, and we use our model to dissect and distill the dynamical mechanisms underlying these network behaviors. Furthermore, we simulate both olfactory and mechanosensory input within our model, showing that model PN responses closely mimic our experimental observations, and we suggest that a slow inhibitory current from LNs to PNs, coupled with the more global nature of mechanosensory input (in comparison to olfactory input) and a glomeruli-spanning LN network that widely distributes inhibition throughout the AL, may be largely responsible for the remarkably disparate AL dynamics we observe in response to olfactory versus mechanosensory signals. Finally, we suggest, using our model, that mechanosensory input may actually somewhat diminish the ability of AL activity to parse and classify a set of ambient environmental odors.

#### 3.1 Biological Implications and Hypotheses

The existence of sensory integration within the AL leads to a natural query: what are the possible biological functions of such bimodality? Insight may be gleaned from two key features of AL responses delineated in this paper: (i) while the PN response to scented puffs at low air speed contains a minimal mechanosensory component and tends to be long-lasting (i.e., not temporally precise), the PN response to scented puffs at high air speed is augmented by a strong mechanosensory component and exhibits a large transient burst (i.e., exhibits more temporal precision); (ii) in general, PNs exhibit larger odor responses in the presence of

significant mechanosensory input (see figures 1 and 7). These starkly disparate PN response patterns in the presence versus absence of a strong mechanosensory signal suggests that the AL may alternate between two mostly distinct dynamic regimes – an odor tracking regime and an odor discrimination regime, respectively.

Odor Tracking Regime: Strong mechanosensory input (e.g., when the insect is mid-flight and actively tracking an odor source) may place the AL within an odor-tracking dynamic regime. Strong mechanosensory input may 'prime' the AL network, allowing an accompanying odor to 'push' the AL into a globally coherent dynamic regime (i.e., a regime of network-wide synchronous activity); when air speed is high, strong and rapidly fluctuating mechanosensory input may induce subthreshold voltage fluctuations across PNs that are tightly correlated and large in amplitude (due to the fact that all PNs receive the same mechanosensory signal), and embedding an odor within the windy flow (causing odor packets to 'ride' atop high-speed air pulses) may then yield widespread PN spiking, tightly correlated spiking across PNs, and greater global coherence and synchrony. Widespread, globally coherent AL activity may then bring full attentional resources to bear on the source-tracking task. Furthermore, strong mechanosensory input (in addition to odor input) may enhance the temporal precision of AL responses (possibly due to both rapid fluctuations in the mechanical input itself as well as AL network mechanisms similar to those encapsulated in figure 8); this may allow the AL to both resolve odor plume dynamics by tracking pulsatile odor delivery (through the transient, precise component of the response) and ascertain odor identity (through the longer-lasting response component).

Odor Discrimination Regime: A relatively small level of mechanosensory input (e.g., when the insect has landed on the surface of or is hovering near a food source) may place the AL within an odor-discrimination dynamic regime (since, without strong, rapidly fluctuating mechanosensory input, tracking odor pulses is less meaningful while fine odor discrimination, enhanced by long-lasting odor inputs, may be a more profitable endeavor). When air speed is low, the minimal mechansensory input may fail to induce large, correlated subthreshold voltage fluctuations across PNs, and accompanying odors may then yield uncorrelated and lower intensity spiking responses across PNs within responsive glomeruli. Additionally, PN responses may be longer-lasting, sacrificing temporal precision for duration. Thus, AL activity is globally unorganized, and is instead dominated by 'patchy' local dynamics unfolding over prolonged time scales, placing the network within a regime devoted to parsing the multitude of environmental odors (rather than tracking rapidly fluctuating odor pulses).

This picture of the biological role of the AL is suggestive, and we therefore propose three overarching, testable hypotheses about the effects of mechanosensory input on AL dynamics: (1) Strong mechanosensory input correlates activity across PNs and glomeruli and results in greater global coherence and synchrony; (2) Strong mechanosensory input enhances the temporal precision and pulse-tracking ability of PN responses; (3) Strong mechanosensory input diminishes the ability of AL activity to discriminate among similar odors (as suggested by figure 9).

Thus, within the insect, strong mechanosensory input may serve as a 'switch' that alternates the AL between odor tracking and odor discrimination dynamic regimes. In the absence of strong mechanosensory input, there is little environmental information to guide tracking of an odor source, and hence the AL may employ locally disconnected, 'patchy', long-lasting dynamics to devote its resources to fine odor discrimination. In the presence of strong mechanosensory input, however, the AL may 'switch' to a more globally coherent regime with temporally precise responses; this allows AL activity to faithfully follow the spatiotemporal dynamics of environmental odor pulses and track an odor source, while sacrificing the ability of network dynamics to finely discriminate among similar odors.

#### 3.2 Sources of Mechanosensory Input to the AL

While our data clearly indicate that AL neurons respond to mechanosensory input in the form of air speed and pressure, this observation leads to a natural query: what are the potential mechanisms by which both mechanosensory and chemosensory information to glomeruli within the AL are conveyed? Olfactory input to the AL is well-known to arise from antennal ORNs, yet the source of mechanosensory input is less certain. However, there are two apparent possibilities that exist. The first may be similar to a mechanism found in vertebrate ORNs. In one study [19], mouse ORNs were shown to respond to both olfactory and mechanical stimuli, and inhibiting adenylyl cyclase completely blocked both types of responses, suggesting that cyclic adenosine monophosphate (cAMP) is involved as a second messenger. Furthermore, knocking out CNG

(cyclic nucleotide-gated channels) eliminated mechanosensitivity. The authors speculated that either some odorant receptors are sensitive to mechanical pressure or a mechanosensor in the membrane might cross-link to the cAMP cascade. In *Manduca sexta*, CNG channels are believed to be similar to those in vertebrates and are directly activated by cAMP and another second messenger, cGMP [37]. The similarities in signal cascade pathways between moth and mouse ORNs may be indicative of physiological similarities as well. The second possibility may be related to the physical proximity of specialized mechanosensitive neurons and ORNs. The somata of bipolar ORNs reside below the base of the sensilum in close physical proximity to one another [34]; the axons of mechanosensory neurons (such as those from the Johnston's organ) travel in the same nerve bundle as the axons of ORNs towards the brain [34, 61], providing opportunities for ephaptic interactions between axons [30, 2, 24]. The ephaptic effects may be further augmented by the fact that invertebrate neurons lack compact myelin sheaths [73].

#### 3.3 Future Directions

Our future work will involve further testing, through combined experimental and computational work, of the hypotheses described above. We will examine the effects of strong mechanosensory input on the correlational structure of PN responses across glomeruli, assessing its effects on global coherence and synchrony within the AL. We will also assess the effects of high air-speed stimuli on the odor discrimination ability of AL activity in order to further refine and probe the mechanisms underlying the modeling results presented in this paper (figure 9).

In particular, we will investigate the ability of PN activity (individually and in aggregate) to track transient odor pulses. Odor stimuli tend to present in nature as a series of discontinuous filaments that occur with higher spatial frequency and in increasing concentration as the odor source is approached. Thus, as a moth travels towards an odor source, it encounters brief pulses of odor that tend to occur at a more rapid rate as the odor source becomes less distant [52]. Additionally, behavioral experiments in which male moths were tested using the female pheromone blend have indicated that intermittent stimuli are more effective at prompting the male moths to exhibit source-seeking behavior than continuous odor plumes [7, 6, 5, 36, 32]. Collectively, these results suggest that the ability of PNs to track stimuli delivered in a pulsatile fashion may be more behaviorally relevant than measuring static responses.

Indeed, experiments show that a series of short (several hundred ms) odor pulses evokes a sequence of corresponding spike trains in activated PNs; each individual pulse produces an I<sub>1</sub> hyperpolarization followed by phase II depolarization and a burst of spikes, with pulse offset eliciting abrupt truncation of spiking activity. The prolonged AHP phase, however, does not manifest until the end of the final pulse in the stimulus train [17, 41]. Intracellular recordings from AL neurons using 50 ms odor pulses show that moth PNs act as low-pass filters of pulse rate (each cell tracks odor pulses with bursts of spikes up to a certain cutoff frequency that varies across PNs). Remarkably, PNs have been found that are capable of tracking up to ten odor pulses per second, while pulse rates exceeding a cell's cutoff frequency elicit responses consisting of tonic firing. Furthermore, the cutoff frequency for pulse tracking is directly related to the amplitude of the  $I_1$  hyperpolarization – PNs that display large  $I_1$  membrane potential deflections are capable of locking to higher pulse rates [14, 21]. The transiency of experimentally observed PN responses to odor pulses tantalizingly mirrors the effects of strong mechanosensory input on AL dynamics explored in this paper. Experimentally assessing the effects of strong mechanosensory input on features of PN pulsetracking ability, while concurrently employing computational modeling to dissect and clarify the underlying dynamical mechanisms, will provide a valuable avenue for investigating the nature, function, and purpose of sensory integration within the AL.

# 4 Methods

#### 4.1 Experimental Procedures

# 4.1.1 Preparation

The dissection procedure was as in a previous publication [40]. In brief, male *Manduca sexta* (Lepidoptera: Sphingidae) moths were restrained with wax in a close-fitting plastic tube with only head protruding out

of the tube. The wings and the rest of the body were capped in the tube to prevent scales from loosening out. The labial palps and proboscis were removed, and a window was cut in the dorsal head capsule. The cibarial pump and other muscles were excised to allow access to the brain. Isolated head preparations were used during recordings. The head preparation was pinned to an algar-coated petri dish, with the ALs oriented anteriorly. The dorsal region of protocerebrum behind an AL was carefully desheathed with a pair of fine forceps. The preparation was superfused with a saline solution (150 mM NaCl, 3 mM CaCl2, 3 mM KCl, 10 mM TES buffer, and 25 mM sucrose, pH 6.9).

#### 4.1.2 Intracellular recording and staining

Sharp microelectrodes were made from borosilicate glass capillaries with filament (1 mm outer diameter, 0.58 mm internal diameter, Sutter Instruments Co., Novato, CA) with a laser puller (P-2000, Sutter Instruments Co., Novato, CA). The tip of the micropipette was filled with a solution of Lucifer Yellow CH (65 mM, Sigma-Aldrich, St. Louis, MO) in 200 mM LiCl, and the shaft with 2 M LiCl; microelectrodes had resistances in the range 100-350 M $\Omega$ . The electrophysiological activity of an impaled neuron to stimulation of the ipsilateral antenna was amplified 10- to 50-fold with an Axoclamp-2A amplifier (Axon Instruments, Molecular Devices, Sunnyvale, CA) coupled to a DC amplifier (LPF 202A, Warner Instruments, Hamden, CT), and digitized at 20 kHz (via Datapack, Run Technologies, Mission Viejo, CA). The medial cluster was targeted in these recordings because most of the pheromone sensitive PNs have their cell bodies in this cluster [26]. After physiological characterization, neurons were injected with Lucifer Yellow by passing hyperpolarizing current (0.21 nA) for 515 min. Upon completion of an experiment, the brain was excised and immersed in 2.5% formaldehyde fixative solution (pH 7.2) overnight at 4° C, dehydrated through a graded series of aqueous ethanol solutions (from 50 to 100%), and cleared with methyl salicylate (Sigma-Aldrich, St. Louis, MO). Cleared brains were imaged as whole mounts with a laser-scanning confocal microscope using a 20X objective lens (Carl Zeiss 510 Meta equipped with a 457-nm Argon laser and a 543-nm Green HeNe laser). Unfortunately, we did not succeed in obtaining any complete fill of these PNs except to observe that their soma are located in the medial cluster. However, these PNs are well described in previous publications [11, 41]. Based on knowledge of the specialized sex-pheromone system of this species, we are confident that our targeted PNs are the same type as those described in previous publications.

#### 4.1.3 Stimulus protocol

Pheromone components, E10-E12-Z14-hexadecatrienal (EEZ) and E10-Z12-hexadecadienal (Bombykal or BAL), were diluted in cyclohexane to a concentration series ranging from 0.1–1000 ng/l and 0.22000 ng/l, respectively. From these stocks, a binary blend was made in the natural 2:1 ratio at concentration of  $10 \text{ ng/}\mu\text{l}$ . One  $\mu\text{l}$  of the blend was deposited on a piece of filter paper that was contained in a 0.5 ml glass syringe. Each syringe was used as a stimulus cartridge to deliver stimuli via a solenoid-controlled air stream. The air stream was supplied from a pressurized building air line, which first passed through a charcoal filter, then a water flask. Before reaching the solenoid, the air stream passed through an air flow meter with mechanical control (AALBORG, Orangeburg, NY). Additionally, a vacuum exhaust funnel was placed behind the preparation to remove odor molecules immediately after each puff. Non-scented air puffs were delivered through empty syringe directly to the antennae without using a constant carrying flow. Stimuli were delivered in train of 5 pulses with duration of 100 ms and interpulse interval of 2 sec. which is well within the range of pulse resolution of these neurons (up to 2 Hz; see Fig. 2 of [44]). The air speed in the delivering line was set at high (about 1 liter per minute) or low (about 0.5 liter per minute), and the air pressure imposed on the solenoid was about 20 psi. In this system it takes about 150 ms for stimulus molecules to reach the antenna. Comparing to a typical wind-tunnel experiment [44] where the wind speed is about 20 cm/sec (or 240 ml/min if realized in a tube of 0.5 cm diameter), the air speeds used in this study are higher but still within a conceivable range. Increasing the air flow speed in scented puffs results in a higher odor flux, i.e. number of molecules per second. Ideally, the flux rate should be kept constant; but that requires extensive further experimentation. For the purposes of the present study, we merely note the differential response to nonscented air puffs at 2 speeds; and since high speed nonscented air puffs yield higher responses than low speed nonscented air puffs (Fig. 1 and Fig. 2), we conclude that at

least some of the increased response to odor-laden puffs at high speed versus low speed is due to increased mechanosensory input.

#### 4.1.4 Data analysis

Time stamps of recorded spikes were extracted within Datapack (Run Technologies, Mission Viejo, CA) and subsequently exported to Neuroexplorer (Nex Technologies, Littleton, MA) to generate peristimulus time histograms (PSTHs) and raster plots. The width of the response window for each neuron was determined by inspecting all PSTHs across the entire dataset. The response windows varied from 0.3 to 0.8 sec. The same width, however, was used for one neuron across all responses. The firing rate during response, i.e. the mean instantaneous firing rate within a response window, was calculated by averaging the inverse of inter-spike intervals (ISI) for all the spikes within the response window.

For each recorded spike trace, a continuous firing rate function was generated by calculating spike rates within a 300 ms sliding window with a step size of 1ms. The background firing rate for a trace was measured over 2500 ms of spontaneous activity. Peak firing rate (in response to a stimulus) over background for a trace was determined as the peak value of the firing rate response to the stimulus divided by background firing rate; the data in figure 2A show averages over 5 trials for each stimulus condition. We set a threshold response value to high flow air (no odor) of 1.5 (i.e., a peak firing rate at least 1.5 times background) to indicate responsiveness to mechanosensory input (this threshold was chosen as a reasonable cutoff based on visual inspection of the data).

Response lengths, as shown in figure 2B, were determined by observing the change in firing rate, relative to background, through time. For each stimulus pulse, we began at the response peak and worked backwards in time until the firing rate over background was 1 or lower (i.e., the firing rate was equivalent to or lower than the background firing rate). This time was considered the start of the response. The end of the response was determined similarly by starting at the response peak and moving forward in time until the firing rate over background returned to 1. Response length was then quantified as end time minus start time. For each stimulus condition, response lengths were averaged over 5 trials to produce the data shown in figure 2B.

The statistical tests carried out in figure 2 employed the Kruskal-Wallis test followed by Turkey-Kramer multiple comparisons, implemented in Matlab.

#### 4.2 Computational Modeling

We constructed a spiking model of the AL network that attempted to attain enough architectural complexity to achieve the complex dynamics of the AL while maintaining enough simplicity to allow for investigation of core mechanistic components. Below, we elaborate on the components and connectivity of our model as well as the details of our analyses of model dynamics.

#### 4.2.1 The Neuron Model

The model was composed of two subclasses of neurons: excitatory, cholinergic PNs and inhibitory, GABAergic LNs. The membrane potential of the  $j^{th}$  PN  $(V_{PN}^{j}(t))$  or the  $j^{th}$  LN  $(V_{LN}^{j}(t))$  were modeled using integrate-and-fire dynamics by the following set of ODEs, which include both intrinsic and synaptic currents:

$$\frac{d}{dt}V_{PN}^{j}(t) = -\frac{1}{\tau_{V}}(V_{PN}^{j} - V_{L}) - g_{SK}^{j}(t)(V_{PN}^{j} - V_{SK}) - g_{stim}^{j}(t)(V_{PN}^{j} - V_{stim}) - g_{exc}^{j}(t)(V_{PN}^{j} - V_{exc}) - g_{inh}^{j}(t)(V_{PN}^{j} - V_{inh}) - g_{slow}^{j}(t)(V_{PN}^{j} - V_{inh})$$

$$\frac{d}{dt}V_{LN}^{j}(t) = -\frac{1}{\tau_{V}}(V_{LN}^{j} - V_{L}) - g_{stim}^{j}(t)(V_{LN}^{j} - V_{stim}) - g_{exc}^{j}(t)(V_{LN}^{j} - V_{exc}) - g_{inh}^{j}(t)(V_{LN}^{j} - V_{inh}) - g_{slow}^{j}(t)(V_{LN}^{j} - V_{inh})$$

PN j in the model was equipped with an intrinsic slow potassium current (SK), and received stimulus-induced input (from external background, odor, and mechanosensory sources), fast excitatory input from other PNs, fast inhibitory input from LNs, and slow inhibitory input from LNs. LN j in the model received stimulus-induced input (from external background, odor, and mechanosensory sources), fast excitatory input from PNs, fast inhibitory input from other LNs, and slow inhibitory input from other LNs. In these equations,  $V_L = 0$ ,  $V_{exc} = V_{stim} = \frac{14}{3}$ , and  $V_{SK} = V_{inh} = -\frac{2}{3}$  (expressed in nondimensional units) represent reversal potentials associated with leakage, excitation, and inhibition respectively. The leakage timescale is given by  $\tau_V = 20$ ms. Upon any neuron reaching a threshold voltage of  $V_{thres} = 1$ , a spike was recorded and its voltage was subsequently reset to  $V_L = 0$  (and held at  $V_L = 0$  for a refractory period of  $\tau_{ref} = 2$ ms). The neuron model was based on a reduced dimensional integrate-and-fire model previously developed in the literature [63], and our network model of the moth AL represents a modification of a prior moth AL model [46] that employed reduced dimensional integrate-and-fire neuron components.

The term  $g_{exc}^{j}(t)$  represents the membrane conductance of neuron j to excitatory synaptic input from PNs, and was modeled as follows:

$$g_{exc}^{j}(t) = \sum_{s \in S} S_{PN} \alpha_{exc}(t|s), \text{ where } \alpha_{exc}(t|s) = \frac{H(t-s)}{\tau_{exc}} e^{-\frac{(t-s)}{\tau_{exc}}},$$

where H(t) is the standard Heaviside Step Function:

$$H(t) = \begin{cases} 1, & t \ge 0 \\ 0, & t < 0 \end{cases}$$

In this equation, S represents the set of all spike times of all PNs presynaptic to neuron j.  $S_{PN}$  is the coupling strength of a network PN to neuron j; we set  $S_{PN} = .01$  if neuron j was a PN, while we set  $S_{PN} = .006$  if neuron j was an LN.  $\alpha_{exc}(t|s)$  is a function with instantaneous rise time and exponential decay time, with time constant  $\tau_{exc} = 2$ ms (whether neuron j was an LN or a PN).

decay time, with time constant  $\tau_{exc} = 2 \text{ms}$  (whether neuron j was an LN or a PN). The other synaptic conductances,  $g_{inh}^{j}(t)$  and  $g_{slow}^{j}(t)$ , as well as the stimulus conductance,  $g_{stim}^{j}(t)$ , were modeled similarly:.

$$g_{inh}^{j}(t) = \sum_{s \in S} S_{inh} \alpha_{inh}(t|s), \text{ where } \alpha_{inh}(t|s) = \frac{H(t-s)}{\tau_{inh}} e^{-\frac{(t-s)}{\tau_{inh}}}$$

$$g_{slow}^{j}(t) = \sum_{s \in S} S_{slow} \alpha_{slow}(t|s), \text{ where } \alpha_{slow}(t|s) = \frac{H(t-s)}{\tau_{slow}} e^{-\frac{(t-s)}{\tau_{slow}}}$$

$$g_{stim}^{j}(t) = \sum_{s \in S} S_{stim} \alpha_{stim}(t|s), \text{ where } \alpha_{stim}(t|s) = \frac{H(t-s)}{\tau_{stim}} e^{-\frac{(t-s)}{\tau_{stim}}}$$

For the  $g_{inh}^j(t)$  and  $g_{slow}^j(t)$  equations, S represents the set of all spike times of all LNs presynaptic to neuron j. For the  $g_{stim}^j(t)$  equation, S represents the set of all spike times of the external input delivered to neuron j; these stimulus-induced spike times arose from simulation of background input, odor input, and mechanosensory input as Poisson processes of incoming spike events (see Stimulus Modeling section below for details). If neuron j was a PN, the coupling strengths were given by  $S_{inh} = 0.0169$ ,  $S_{slow} = 0.0338$ , and  $S_{stim} = 0.004$ , while if neuron j was an LN, the coupling strengths were given by  $S_{inh} = 0.015$ ,  $S_{slow} = 0.04$ , and  $S_{stim} = 0.0031$ . The fast inhibition and stimulus timescales were comparable to excitation, with  $\tau_{inh} = \tau_{stim} = 2$ ms, while the slow inhibition time scale was dramatically slower, with  $\tau_{slow} = 750$ ms (whether neuron j was a PN or an LN).

Finally, the SK current is an intrinsic slow potassium current, displayed by only PNs, that activates upon spiking and serves to curb further spiking activity. Rather than an instantaneous jump, the rise time of the SK current was modeled as sigmoidal; this non-instantaneous rise time allowed PNs to potentially emit multiple spikes prior to suppression of firing activity by the SK current. The SK current for PN j was modeled as follows:

$$g_{SK}^{j}(t) = \sum_{s \in S} S_{SK} \beta(t|s)$$

$$\beta(t|s) = \begin{cases} \frac{H(t-s)}{\tau_{SK}} \frac{e^{\frac{5((t-s)-\tau_{rise})}{\tau_{rise}}}}{\frac{5((t-s)-\tau_{rise})}{\tau_{rise}}}, & t \le s + 2\tau_{rise} \\ \frac{1+e^{\frac{\tau_{rise}}{\tau_{rise}}}}{\tau_{SK}}, & t > s + 2\tau_{rise} \end{cases}$$

S represents the set of all firing times of PN j. The strength  $S_{SK}$  of the SK current was a randomly determined, but fixed, parameter, and hence varied from PN to PN; the value of  $S_{SK}$  for PN j was drawn from a normal distribution with mean  $\mu=.5$  and standard deviation  $\sigma=.2$ . While rare, it was possible for  $S_{SK}$  to be negative with this distribution, so any negative value for  $S_{SK}$  was manually set to 0.  $\tau_{SK}=250$ ms, and the rise of the SK current was modeled as sigmoidal with a half-rise time of  $\tau_{rise}=25$ ms.

#### 4.2.2 Network Architecture

Our AL model consisted of 6 glomeruli, with each glomerulus consisting of 10 PNs and 6 LNs; connectivity within glomeruli was dense in comparison with relatively sparse connectivity across glomeruli. Synaptic connections within the model were randomly determined but fixed, with the probability of a synaptic connection varying within and across glomeruli and dependent on cell type. Within a glomerulus, the PN $\rightarrow$ PN, PN $\rightarrow$ LN, LN $\rightarrow$ PN, LN $\rightarrow$ LN connection probabilities were given by 0.75, 0.75, 0.38, 0.25, respectively. Long-range connections (i.e., connections across glomeruli) were mediated exclusively by LN $\rightarrow$ PN synapses, and the cross-glomerular LN $\rightarrow$ PN connection probability was given by 0.38.

It is worth mentioning that the model itself is quite robust, with the exact input parameters provided not essential to producing reasonable behavior. Rather, we found that combinations of parameters, and hence the relative strength of disparate network components, were important for producing realistic behavior. For example, we found that slow inhibition must be sufficiently strong, relative to stimulus-induced inputs, to suppress PN spiking if the global LN network was activated, yet not so strong as to silence PN activity upon only focal activation of a few glomeruli. Likewise, we found that the strength of the SK current must fall within a broad range of values, relative to the strength of stimulus-induced inputs and LN inhibition, with the lower end of this range yielding homogeneous PN spiking activity and the higher end of this range yielding burst-like PN behavior. Hence, our parameter choices represent a single point drawn from a relatively large cloud (in multidimensional parameter space) of parameter combinations that produce physiologically reasonable behavior.

#### 4.2.3 Stimulus Modeling

Rather than explicitly modeling the behavior of ORNs or the cells responsible for mechanosensory sensory inputs, input to each cell within the network was modeled as a Poisson process of incoming spikes. An incoming spike to neuron j within the network was modeled as an instantaneous jump in  $g_{stim}^j(t)$  of size .004 if neuron j was a PN, or .0031 if neuron j was an LN, followed by exponential decay with time constant  $\tau = 2$ ms (whether neuron j was a PN or an LN). Each cell had three potential sources of input; all cells received a background rate of  $\lambda_{back} = 3.6$  spikes/ms, while odor input (simulating the presence of a single odor) was delivered at a maximum rate of  $\lambda_{max}^{max} = 3.6$  spikes/ms and mechanosensory input was delivered at a maximum rate of  $\lambda_{mech}^{max} = 1.8$  spikes/ms. The total rate of incoming spikes for the  $j^{th}$  cell was therefore given by:

$$\lambda_{tot}^{j}(t) = \lambda_{back} + \lambda_{odor}^{j}O^{j}(t) + \lambda_{mech}^{j}M^{j}(t),$$

where  $O^{j}(t)$  and  $M^{j}(t)$  are functions that range between 0 and 1 and serve to model the temporal dynamics of odor and mechanosensory input pulses, respectively.

To simulate background AL activity, we set  $\lambda^j_{odor} = 0$  and  $\lambda^j_{mech} = 0$  for all j. To simulate a single odor (without simulation of mechanosensory input) presented at time  $t_{on}$  and removed at time  $t_{off}$ , we sent odor-induced input to all cells within 3 out of 6 model glomeruli (with the glomerular subset signifying odor identity); we therefore set  $\lambda^j_{odor} = 0$  if cell j belonged to an unstimulated glomerulus and  $\lambda^j_{odor} = \lambda^{max}_{odor}$  if cell j belonged to a stimulated glomerulus, and set  $\lambda^j_{mech} = 0$  for all j. To simulate a pulse of mechanosensory input (without an accompanying olfactory stimulus) from time  $t_{on}$  to time  $t_{off}$ , we set  $\lambda^j_{odor} = 0$  and

 $\lambda_{mech}^{j} = \lambda_{mech}^{max}$  for all j. Hence, within the model, olfactory input stimulated a focal glomerular subset, while mechanosensory input represented a global signal delivered to the entirety of the AL.

In addition to simulating olfactory and mechanosensory input in isolation, we also simulated the two in combination. To simulate a stimulus pulse (from time  $t_{on}$  to time  $t_{off}$ ) consisting of a single odor accompanied by a mechanosensory signal, we employed two distinct paradigms – the additive sensory integration and the normalized sensory integration paradigms. In the additive sensory integration paradigm, we set  $\lambda^j_{odor} = 0$  if cell j belonged to a glomerulus not responsive to the odor and  $\lambda^j_{odor} = \lambda^{max}_{odor}$  if cell j belonged to a glomerulus activated by the odor, and set  $\lambda^j_{mech} = \lambda^{max}_{mech}$  for all j. In the normalized sensory integration paradigm, we set  $\lambda^j_{odor} = 0$  if cell j belonged to a glomerulus not responsive to the odor and  $\lambda^j_{odor} = \frac{1}{2}\lambda^{max}_{mech}$  if cell j belonged to a glomerulus activated by the odor, and set  $\lambda^j_{mech} = \frac{1}{2}\lambda^{max}_{mech}$  for all j. Hence, the additive paradigm simply 'added' together the isolated olfactory and mechanosensory signals, while the normalized paradigm scaled the two signals in order to maintain a similar overall level of excitation sent to the AL network in comparison to the cases of olfactory input or mechanosensory input in isolation.

Finally, to simulate two odors simultaneously (as in figure 9), we simply 'added' the inputs resulting from the two odors in isolation. In other words, we set  $\lambda^j_{odor}=0$  if cell j belonged to a glomerulus stimulated by neither odor,  $\lambda^j_{odor}=\lambda^{max}_{odor}$  if cell j belonged to a glomerulus stimulated by only 1 of the 2 odors, and  $\lambda^j_{odor}=2\lambda^{max}_{odor}$  if cell j belonged to a glomerulus stimulated by both odors.

The function  $O^{j}(t)$  represents the temporal dynamics of the olfactory component of a stimulus pulse beginning at time  $t_{on}$  and ending at time  $t_{off}$  (with  $t_{off} - t_{on} = 1000 \text{ms} - \text{i.e.}$ , stimulus pulses were modeled as having a 1 sec duration).  $O^{j}(t) = 0$  for  $t < t_{on}$ ; at time  $t_{on}$ ,  $O^{j}(t)$  increases from 0 to 1 with a prescribed rise time, while for  $t > t_{off}$ ,  $O^{j}(t)$  decreases from 1 to 0 with a prescribed decay time. If neuron j was a PN, rise was sigmoidal with a half-rise time of  $\tau_{rise} = 35 \text{ms}$ , while decay was exponential with  $\tau_{decay} = 384 \text{ms}$ :

$$\text{If } j \text{ is a PN, } O^{j}(t) = \begin{cases} H(t - t_{on}) \frac{e^{\frac{5(((t - t_{on}) - \tau_{rise})}{\tau_{rise}}}}{\frac{5((t - t_{on}) - \tau_{rise})}{\tau_{rise}}}, & t \leq t_{on} + 2\tau_{rise} \\ 1, & t_{on} + 2\tau_{rise} < t \leq t_{off} \\ e^{\frac{-(t - t_{off})}{\tau_{decay}}}, & t_{off} < t \end{cases}$$

If neuron j was a LN, rise was instantaneous, while decay was exponential with  $\tau_{decay} = 384$ ms:

If 
$$j$$
 is an LN,  $O^{j}(t) = \begin{cases} H(t - t_{on}), & t \leq t_{off} \\ e^{\frac{-(t - t_{off})}{\tau_{decay}}}, & t_{off} < t \end{cases}$ 

For  $O^{j}(t)$  we chose a sigmoidal rise time for PNs versus an instantaneous rise time for LNs in order to capture the brief PN hyperpolarization that occurs at odor onset (the  $I_1$  phase of the odor response, described further in the *Results* section). A slightly longer rise time for PNs ensured that the synchronized burst of LN spikes that occurred at odor onset was strong enough to hyperpolarize PNs for a brief period prior to the rise of the odor-induced current to PNs. While the  $I_1$  phase can be achieved in several ways (e.g., strengthening fast inhibition from LNs to PNs, increasing the strength of the odor-induced current to LNs, or decreasing the strength of the odor-induced current to PNs), the exact dynamics underlying the  $I_1$  phase are not known, and hence in our model we chose to employ a differential rise time of the odor-induced current to PNs versus LNs.

Similarly, the function  $M^{j}(t)$  represents the temporal dynamics of the mechanosensory component of a stimulus pulse beginning at time  $t_{on}$  and ending at time  $t_{off}$  ( $t_{off} - t_{on} = 1000 \text{ms}$ ).  $M^{j}(t) = 0$  for  $t < t_{on}$ ; at time  $t_{on}$ ,  $M^{j}(t)$  increases from 0 to 1 with a prescribed rise time, while for  $t > t_{off}$ ,  $M^{j}(t)$  decreases from 1 to 0 with a prescribed decay time. If neuron j was a PN, rise was instantaneous and decay was exponential with  $\tau_{decay} = 384 \text{ms}$ :

If 
$$j$$
 is a PN,  $M^{j}(t) = \begin{cases} H(t - t_{on}), & t \leq t_{off} \\ e^{\frac{-(t - t_{off})}{\tau_{decay}}}, & t_{off} < t \end{cases}$ 

If neuron j was a LN,  $\tau_{rise} = 300 \text{ms}$  and  $\tau_{decay} = 384 \text{ms}$ :

$$\text{If } j \text{ is an LN, } M^{j}(t) = \begin{cases} H(t - t_{on}) \frac{e^{\frac{5((t - t_{on}) - \tau_{rise})}{\tau_{rise}}}}{1 + e^{\frac{5((t - t_{on}) - \tau_{rise})}{\tau_{rise}}}}, & t \leq t_{on} + 2\tau_{rise} \\ 1, & t_{on} + 2\tau_{rise} < t \leq t_{off} \\ e^{\frac{-(t - t_{off})}{\tau_{decay}}}, & t_{off} < t \end{cases}$$

We included a significantly longer rise time for mechanosensory input to LNs, relative to that for PNs, in order to ensure that global LN inhibition at the inception of a stimulus pulse (mediated by fast inhibitory synapses) was not overwhelmingly powerfully enough to prevent PN spiking altogether, and that substantial suppression of PN spiking must await the lengthy activation time of slow inhibitory synapses. This assumption, however, is not necessarily required to obtain physiologically reasonable dynamics – for example, weakening fast inhibitory synapses from LNs to PNs or strengthening slow inhibition while reducing the density of LN→PN synapses can yield similar dynamical effects without such a disparity in rise times. Since the dynamics of mechanosensory input to AL cells has not yet been studied within the experimental literature, we (somewhat arbitratrily, due to ignorance of the actual physiological mechanism at play) chose to include this mechanism of a disparity in rise times to ensure robust PN spiking at stimulus onset. However, we note that including a disparity in rise times does not affect the basic dynamical behavior of the model, other than delaying suppression of PN spiking at stimulus onset.

#### 4.2.4 Simulation and Data Analysis

Means and standard deviations were taken over 100 trials. Normalized firing rates (as in figure 8) were determined by dividing the firing rate during a period of interest (in our case, the last 500ms of an odor pulse) by the firing rate during 1 second of background activity (both averaged over 100 trials). Thus, a normalized firing rate greater than 1 represents enhanced spiking activity (over background) while a normalized firing rate less than 1 represents reduced spiking activity (relative to background).

Odor discrimination rates within the model (as in figure 9) were determined using a linear classification scheme. To calculate the time-dependent ability of the network to discriminate among n stimuli, we split the total simulation time into nonoverlapping 10ms time bins; for stimulus  $i \in [1, n]$  and time bin k, we constructed a template for stimulus i in time bin k as the 60-dimensional vector of PN firing rates within time bin k averaged over 100 trials of stimulus i presentation. This yielded a total of 100n odor trials and n odor templates for time bin k. For an individual stimulus trial (for, say, stimulus  $l \in [1, n]$ ), we designated the trial as 'correctly classified' within time bin k if the Euclidean distance between the 60-dimensional vector of PN firing rates for that trial and each of the n odor templates was smallest for the template for odor l; otherwise, we designated the trial as 'incorrectly classified'. The classification rate of the network in time bin k was then determined as the number of 'correctly classified' odor trials within time bin k divided by 100n.

Numerical simulations were carried out using the Euler Method with a time step of  $\Delta t = 0.1$ ms. Model code was written in C++ with data analysis and plotting carried out in Matlab. Model code is available at https://gitlab.com/HarrisonTuckmanWM/antennal-lobe-model-2-0.

# Acknowledgements

We would like to thank John G. Hildebrand (Department of Neuroscience, University of Arizona), who provided the laboratory space and equipment for the experimental component of this work.

# References

- [1] B. Ache and J. Young. Olfaction: Diverse species, conserved principles. Neuron, 48:417–430, 2005.
- [2] C. Anastassiou, R. Perin, H. Markram, and C. Koch. Ephaptic coupling of cortical neurons. *Nat Neurosci*, 14:217–223, 2011.

- [3] N. Ando and R. Kanzaki. A simple behaviour provides accuracy and flexibility in odour plume tracking the robotic control of sensory-motor coupling in silkmoths. *J Exp Biol*, 218:3845–3854, 2015.
- [4] K. Baker, G. Vasan, A. Gumaste, V. Pieribone, and J. Verhagen. Spatiotemporal dynamics of odor responses in the lateral and dorsal olfactory bulb. PLoS Biology, 17:e3000409, 2019.
- [5] T. Baker. Sex pheromone communication in the lepidoptera: new research progress. Experientia, 45:248–262, 1989.
- [6] T. Baker, B. Hansson, T. Lofstedt, and J. Lofqvist. Adaptation of antennal neurons in moths is associated with cessation of pheromone-mediated upwind flight. *Proc Natl Acad Sci USA*, 85:9826– 9830, 1988.
- [7] T. Baker, M. Willis, K. Haynes, and P. Phelan. A pulsed cloud of sex pheromone elicits upwind flight in male moths. *Physiol Entomol*, 10:257–265, 1985.
- [8] A. Brinkmann and D. Schild. One special glomerulus in the olfactory bulb of xenopus laevis tadpoles integrates a broad range of amino acids and mechanical stimuli. *J Neurosci*, 36:10978–10989, 2016.
- [9] R. Carde and M. Willis. Navigational strategies used by insects to find distant, wind-borne sources of odor. J Chem Ecol, 34:854–866, 2008.
- [10] T. Christensen and J. Hildebrand. Functions, organization and physiology of the olfactory pathways in the lepidopteran brain. *In: Arthropod Brain. It's Evolution, Development, Structure and Functions.* (Gupta AP, ed). New York: Wiley, pages 457–484, 1987.
- [11] T. Christensen and J. Hildebrand. Male-specific, sex-pheromone-selective projection neurons in the antennal lobes of the moth manduca sexta. J Comp Physiol A, 160:553–569, 1987.
- [12] T. Christensen and J. Hildebrand. Frequency coding by central olfactory neurons in the sphinx moth manduca sexta. Chem Senses, 13:123–130, 1988.
- [13] T. Christensen and J. Hildebrand. Representation of sex-pheromonal information in the insect brain. In: Doving KB (ed) Proc Xth Internatl Symp Olfaction and Taste (ISOT X). Graphic Communication Systems, Oslo, pages 142–150, 1990.
- [14] T. Christensen and J. Hildebrand. Coincident stimulation with pheromone components improves temporal pattern resolution in central olfactory neurons. J Neurophysiol, 77:775–781, 1997.
- [15] T. Christensen, V. Pawlowski, H. Lei, and J. Hildebrand. Multi-unit recordings reveal context-dependent modulation of synchrony in odor-specific neural ensembles. *Nat Neurosci*, 3:927–931, 2000.
- [16] T. Christensen, B. Waldrop, I. Harrow, and J. Hildebrand. Local interneurons and information processing in the olfactory glomeruli of the moth manduca sexta. J Comp Physiol A, 173:385–399, 1993.
- [17] T. Christensen, B. Waldrop, and J. Hildebrand. Multitasking in the olfactory system: context-dependent responses to odors reveal dual gaba-regulated coding mechanisms in single olfactory projection neurons. *J Neurosci*, 18:5999–6008, 1998.
- [18] A. Froese, P. Szyszka, and R. Menzel. Effect of gabaergic inhibition on odorant concentration coding in mushroom body intrinsic neurons of the honeybee. *J Comp Physiol*, 200:183–195, 2014.
- [19] X. Grosmaitre, L. Santarelli, J. Tan, M. Luo, and M. Ma. Dual functions of mammalian olfactory sensory neurons as odor detectors and mechanical sensors. *Nat Neurosci*, 10:348–354, 2007.
- [20] Q. Han, B. Hansson, and S. Anton. Interactions of mechanical stimuli and sex pheromone information in antennal lobe neurons of a male moth, spodoptera littoralis. *J Comp Physiol A Neuroethol Sens Neural Behav Physiol.*, 191:521–528, 2005.

- [21] T. Heinbockel, T. Christensen, and J. Hildebrand. Temporal tuning of odor responses in pheromone-responsive projection neurons in the brain of the sphinx moth manduca sexta. J Comp Neurol, 409:1–12, 1999.
- [22] J. Hildebrand, L. Hall, and B. Osmond. Distribution of binding sites for <sup>125</sup>i-labeled alphabungarotoxin in normal and deafferented antennal lobes of manduca sexta. Proc Natl Acad Sci USA, 76:499–503, 1979.
- [23] J. Hildebrand and G. Shepherd. Mechanisms of olfactory discrimination: Converging evidence for common principles across phyla. Annu Rev Neurosci, 20:595–631, 1997.
- [24] N. Hillier and N. Vickers. Mixture interactions in moth olfactory physiology: examining the effects of odorant mixture, concentration, distal stimulation, and antennal nerve transection on sensillar responses. *Chemical Senses*, 36:93–108, 2011.
- [25] U. Homberg, T. Christensen, and J. Hildebrand. Structure and function of the deutocerebrum in insects. Annu Rev Entomol., 34:477–501, 1989.
- [26] U. Homberg, R. Montague, and J. Hildebrand. Anatomy of antenno-cerebral pathway in the brain of the sphinx moth manduca sexta. Cell Tissue Res, 254:255–281, 1988.
- [27] S. Hoskins, U. Homberg, T. Kingan, T. Christensen, and J. Hildebrand. Immunocytochemistry of gaba in the antennal lobes of the sphinx moth manduca sexta. Cell Tissue Res, 244:243–252, 1986.
- [28] R. Iwata, H. Kiyonari, and T. Imai. Mechanosensory-based phase coding of odor identity in the olfactory bulb. *Neuron*, 96:1139–1152, 2017.
- [29] A. Jarman. Studies of mechanosensation using the fly. Human Mol Gen, 11:1215–1218, 2002.
- [30] J. Jefferys. Nonsynaptic modulation of neuronal activity in the brain: electric currents and extracellular ions. *Physiological Reviews*, 75:689–723, 1995.
- [31] J. Joerges, A. Kuttner, G. Galizia, and R. Menzel. Representations of odours and odour mixtures visualized in the honeybee brain. *Nature*, 387:285–288, 1997.
- [32] K. Kaissling and E. Kramer. Sensory basis of pheromone-mediated orientation in moths. Verh Dtsch Zool Ges, 83:109–131, 1990.
- [33] R. Kanzaki, E. Arbas, N. Strausfeld, and J. Hildebrand. Physiology and morphology of projection neurons in the antennal lobe of the male moth manduca sexta. J Comp Physiol A, 165:427–453, 1989.
- [34] T. Keil. Fine structure of the pheromone-sensitive sensilla on the antenna of the hawkmoth, manduca sexta. TISSUE CELL, 21:139–151, 1989.
- [35] T. Kingan and J. Hildebrand. Gamma-aminobutyric acid in the central nervous system of metamorphosing and mature manduca sexta. Insect Biochem, 15:667–675, 1985.
- [36] E. Kramer. Attractivity of pheromone surpassed by time-patterned application of two nonpheromone compounds. *J Insect Behav*, 5:83–97, 1992.
- [37] S. Krannich and M. Stengl. Cyclic nucleotide-activated currents in cultured olfactory receptor neurons of the hawkmoth manduca sexta. Journal of Neurophysiology, 100:2866–2877, 2008.
- [38] M. Larsson and B. Hansson. Receptor neuron responses to potential sex pheromone components in the caddisfly rhyacophila nubila (trichoptera: Rhyacophilidae). *J Insect Physiol*, 44:189–196, 1998.
- [39] J. Lee and N. Strausfeld. Structure, distribution and number of surface sensilla and their receptor cells on the olfactory appendage of the male moth manduca sexta. J Neurocytol, 19:519–538, 1990.
- [40] H. Lei, H. Chiu, and J. Hildebrand. Responses of protocerebral neurons in manduca sexta to sexpheromone mixtures. J Comp Physiol A Neuroethol Sens Neural Behav Physiol, 199:997–1014, 2013.

- [41] H. Lei, T. Christensen, and J. Hildebrand. Local inhibition modulates odor-evoked synchronization of glomerulus-specific output neurons. *Nat Neurosci*, 5:557–565, 2002.
- [42] H. Lei, T. Christensen, and J. Hildebrand. Spatial and temporal organization of ensemble representations for different odor classes in the moth antennal lobe. *J Neurosci*, 24:11108–11119, 2004.
- [43] H. Lei, C.E. Reisenman, C.H. Wilson, P. Gabbur, and J.G. Hildebrand. Spiking patterns and their functional implications in the antennal lobe of the tobacco hornworm manduca sexta. PLosONE, 6:e23382, 2011. doi: 10.1371/journal.pone.0023382.
- [44] H. Lei, J. Riffell, S. Gage, and J. Hildebrand. Contrast enhancement of stimulus intermittency in a primary olfactory network and its behavioral significance. *J Biol*, 8:21, 2009.
- [45] H. Lei and N. Vickers. Central processing of natural odor mixtures in insects. *J Chem Ecol*, 34:915–927, 2008.
- [46] H. Lei, Y. Yu, S. Zhu, and A.V. Rangan. Intrinsic and network mechanisms constrain neural synchrony in the moth antennal lobe. *Front. Physiol.*, 7:80, 2016. doi:10.3389/fphys.2016.00080.
- [47] B. Malnic, J. Hirono, T. Sato, and L. Buck. Combinatorial receptor codes for odors. Cell, 96:713–723, 1999.
- [48] A. Mamiya and M. Dickinson. Antennal mechanosensory neurons mediate wing motor reflexes in flying drosophila. *J Neurosci.*, 35:7977–7991, 2015.
- [49] S. Matsumoto and J. Hildebrand. Olfactory mechanisms in the moth manduca sexta: response characteristics and morphology of central neurons in the antennal lobes. Proc R Soc Lond B, 213:249–277, 1981.
- [50] A. Mercer and J. Hildebrand. Developmental changes in the density of ionic currents in antennal-lobe neurons of the sphinx moth, manduca sexta. J Neurophysiol, 87:2664–1675, 2002.
- [51] A. Mercer and J. Hildebrand. Developmental changes in the electrophysiological properties and response characteristics of *manduca* antennal-lobe neurons. *J Neurophysiol*, 87:2650–2663, 2002.
- [52] J. Murlis, J. Elkinton, and R. Carde. Odor plumes and how insects use them. Ann Rev Entomol, 37:505–532, 1992.
- [53] J. Murlis and C. Jones. Fine-scale structure of odor plumes in relation to insect orientation to distant pheromone and other attractant sources. *Physio Ento*, 6:71–86, 1981.
- [54] M. Ng, R. Roorda, S. Lima, B. Zemelman, P. Morcillo, and G. Miesenbock. Transmission of olfactory information between three populations of neurons in the antennal lobe of the fly. *Neuron*, 36:463–474, 2002.
- [55] K. Park and A. Cork. Electrophysiological responses of antennal receptor neurons in female australian sheep blowflies, lucilia cuprina, to host odours. *Journal of Insect Physiology*, 45:85–91, 1999.
- [56] Z. Pasternak, F. Bartumeus, and F. Grasso. Levy-taxis: a novel search strategy for finding odor plumes in turbulent flow-dominated environments. *J PhyA-Math Theo*, 42, 2009.
- [57] P. Patella and R. Wilson. Functional maps of mechanosensory features in the drosophila brain. *Current Biology*, 28:1189–1203, 2018.
- [58] P. et al. Pyk. An artificial moth: Chemical source localization using a robot based neuronal model of moth optomotor anemotactic search. *Auto rob*, 20:197–213, 2006.
- [59] C. Reisenman, T. Christensen, W. Francke, and J. Hildebrand. Enantioselectivity of projection neurons innervating identified olfactory glomeruli. *J Neurosci*, 24:2602–2611, 2004.

- [60] M. Sanchez and K. Kaissling. Inhibitory and excitatory effects of iodobenzene on the antennal benzoic acid receptor cells of the female silk moth bombyx mori l. *Chem Senses*, 30:435–442, 2005.
- [61] S. Sane, A. Dieudonne, M. Willis, and T. Daniel. Antennal mechanosensors mediate flight control in moths. Science, 315:863–866, 2007.
- [62] A. Silbering and C. Galizia. Processing of odor mixtures in the drosophila antennal lobe reveals both global inhibition and glomerulus-specific interactions. *J Neurosci*, 27:11966–11977, 2007.
- [63] L. Tao, M. Shelley, D. McLaughlin, and R. Shapley. An egalitarian network model for the emergence of simple and complex cells in visual cortex. *Proc Natl Acad Sci USA*, 101:366, 2004.
- [64] M. Vergassola, E. Villermaux, and B. Shraiman. 'infotaxis' as a strategy for searching without gradients. Nature, 445:406–409, 2007.
- [65] N. Vickers. Mechanisms of animal navigation in odor plumes. Biol Bull, 198:203-212, 2000.
- [66] N. Vickers and T. Baker. Reiterative responses to single strands of odor promote sustained upwind flight and odor source location by moths. *Proc Nat Aca Sci USA*, 91:5756–5760, 1994.
- [67] N. Vickers and T. Christensen. A combinatorial model of odor discrimination using a small array of contiguous, chemically defined glomeruli. *Ann NY Acad Sci*, 855:514–516, 1998.
- [68] N. Vickers, T. Christensen, and J. Hildebrand. Combinatorial odor discrimination in the brain: Attractive and antagonistic odor blends are represented in distinct combinations of uniquely identifiable glomeruli. J Comp Neurol, 400:35–36, 1998.
- [69] B. Waldrop, T. Christensen, and J. Hildebrand. Gaba-mediated synaptic inhibition of projection neurons in the antennal lobes of the sphinx moth, manduca sexta. J Comp Physiol A, 161:23–32, 1987.
- [70] J. Wang, A. Wong, J. Flores, L. Vosshall, and R. Axel. Two-photon calcium imaging reveals an odor-evoked map of activity in the fly brain. *Cell*, 112:271–282, 2003.
- [71] A. Whitehead and J. Larsen. Ultrastructure of the contact chemoreceptors of apis mellifera l. (hymenoptera: Apidae). Int J Insect Morphol Embryol, 5:301–315, 1976.
- [72] N. Yamagata, M. Schmuker, P. Szyszka, M. Mizunami, and R. Mensel. Differential odor processing in two olfactory pathways in the honeybee. Frontiers in Systems Neuroscience, 3:doi:10.3389, 2009.
- [73] B. Zalc. The acquisition of myelin: An evolutionary perspective. Brain Research, 1641:4–10, 2016.

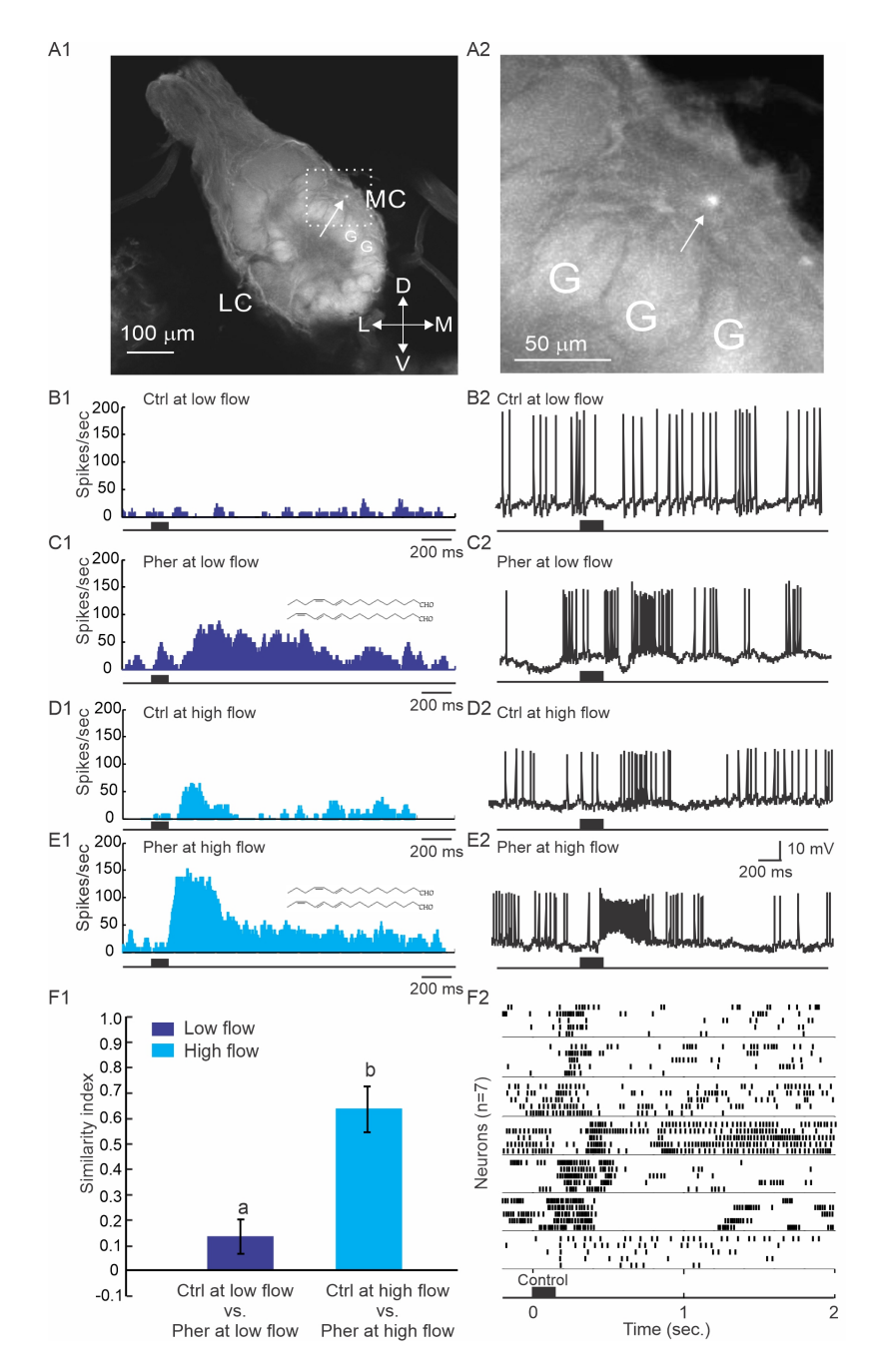


Figure 1: Figure 1. Mechanosensory input shapes PN response patterns. (A) Confocal microscopic images show a single PN cell body (arrow) located in the medial cluster, labeled with Lucifer yellow fluorescent dye. The square in A1 is magnified in A2. MC: medial cluster of cell bodies; LC: lateral cluster of cell bodies; G: glomerulus; D: dorsal; V: ventral; L: lateral; M: medial. (B-E) Response of a representative PN to consecutive non-scented air puffs or pheromone-infused air puffs. While responses to pheromone-infused air puffs are stronger, non-scented air puffs induce robust responses as well. The peristimulus histograms (PSTHs) were based on responses to 5 puffs of non-scented air (B1) and pheromone blend (C1) at low air speed, and responses to the same stimuli but at high air speed (D1, E1). Examples of the raw intracellular spike traces show response to single stimulus puff under each air speed-stimulus scenario (B2, C2, D2, E2). Note that a non-scented air puff at high speed evoked a response pattern similar to that evoked by pheromone at high puffing speed. The correlation coefficient between D1 and E1 is 0.69 whereas the correlation coefficient between B1 and C1 is only 0.19. (F) High flow speed produced more similar response patterns between the control and pheromone treatment (cyan bar in F1, mean $\pm$ SE) than the low flow speed did (blue bar in F1, mean $\pm$ SE) (Mann-Whitney U test, p < 0.0001, n=7, Panel F1). Raster plots show diverse responses to non-scented air puffs at high flow rate (F2). From B to E, stimulus delivery started at time zero and lasted for 200 ms. The black bar below each histogram indicates the duration of one stimulus pulse, but the histogram is averaged across five pulses.

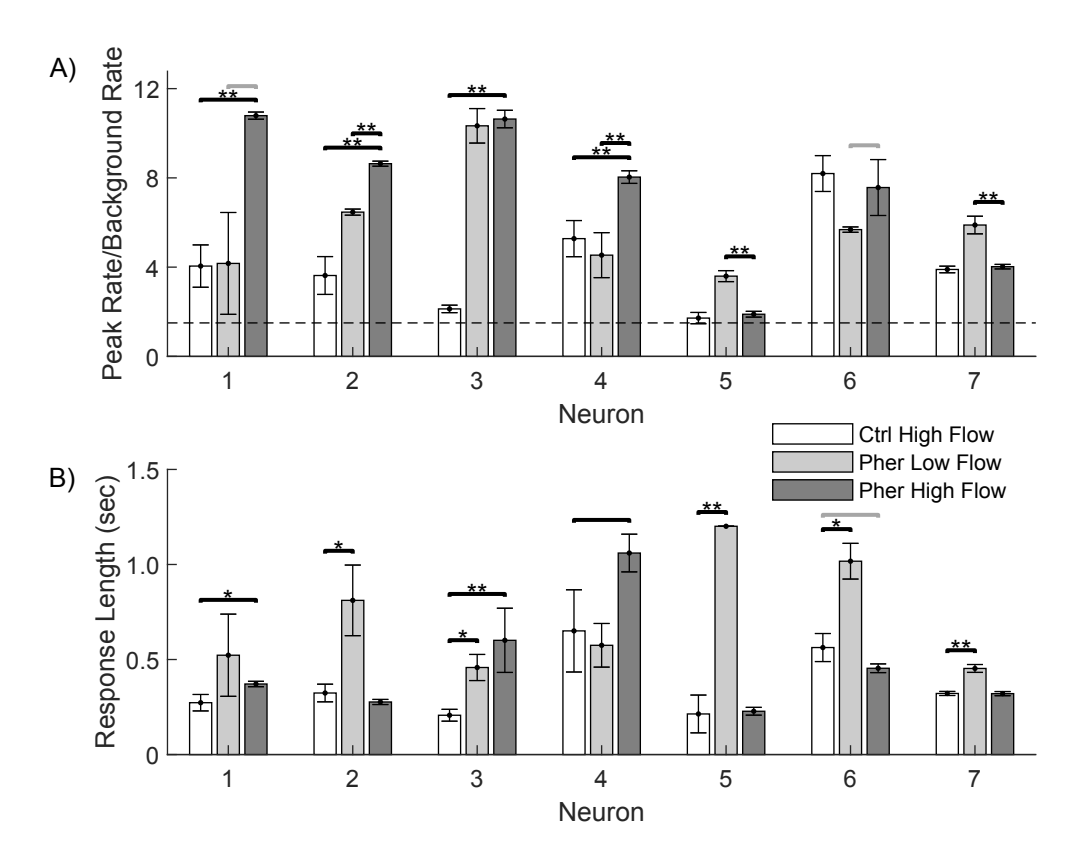


Figure 2: Figure 2. Response strengths and durations of the 7/9 recorded cells that were deemed responsive to mechanosensory input; responses to strong mechanosensory input alone (Control High Flow), odor with minimal mechanosesory input (Pheromone Low Flow), and odor concurrently with strong mechanosensory input (Pheromone High Flow) are shown. (A) Peak firing rate response of each cell divided by the background firing rate for the cell. A cell was deemed responsive to mechanosensory input if the Control High Flow condition yieled a response exceeding 1.5X background; this threshold is shown by the dashed line. (B) Total duration of a neuron's response to each stimulus condition. Data are averaged over 5 trials; error bars show mean  $\pm$  SEM. Gray bar with no stars indicates p < 0.15; black bar with no stars indicates p < 0.15; black bar with one stars indicates p < 0.15; black bar with one stars indicates p < 0.15; black bar with one stars indicates p < 0.15; black bar with one stars indicates p < 0.15; black bar with one stars indicates p < 0.15; black bar with one stars indicates p < 0.15; black bar with one stars indicates p < 0.15; black bar with one stars indicates p < 0.15; black bar with one stars indicates p < 0.15; black bar with one stars indicates p < 0.15; black bar with one stars indicates p < 0.15; black bar with one stars indicates p < 0.15; black bar with one stars indicates p < 0.15; black bar with one stars indicates p < 0.15; black bar with one stars indicates p < 0.15; black bar with one stars indicates p < 0.15; black bar with one stars indicates p < 0.15; black bar with one stars indicates p < 0.15; black bar with one stars indicates p < 0.15; black bar with one stars indicates p < 0.15; black bar with one stars indicates p < 0.15; black bar with one stars indicates p < 0.15; black bar with one stars indicates p < 0.15; black bar with one stars indicates p < 0.15; black bar with one stars indicates p < 0.15; black bar with one stars i

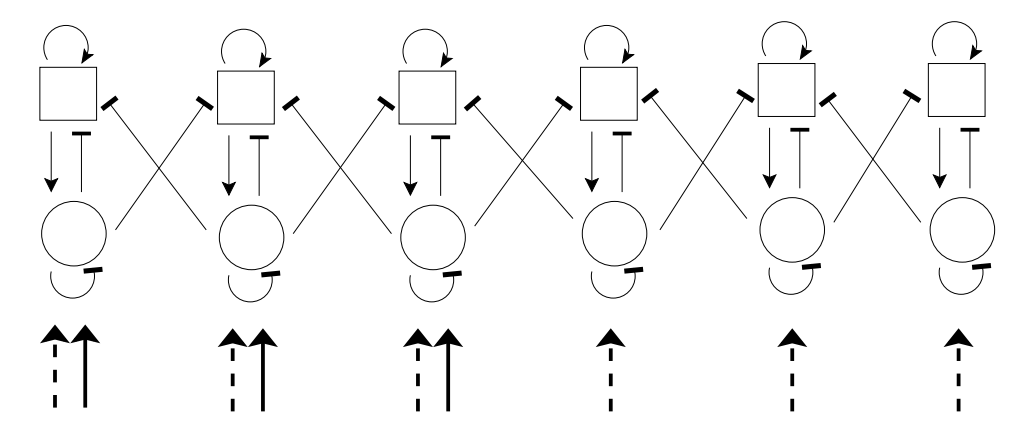


Figure 3: Figure 3. Schematic of model AL network. Each column represents a glomerulus; squares represent PNs (10 per glomerulus) and circles represent LNs (6 per glomerulus). Arrow heads indicate excitation, while bar heads indicate inhibition. Within a glomerulus, all cell types form synapses with each other (with cell type-specific connection probabilities), while glomerular cross-talk is mediated only via LN $\rightarrow$ PN synapses. An odor is simulated via delivery of excitatory stimulus current to all cells within a subset of three glomeruli (solid incoming arrows), while strong mechanosensory input is simulated via delivery of excitatory stimulus current to all cells within all glomeruli (dashed incoming arrows).

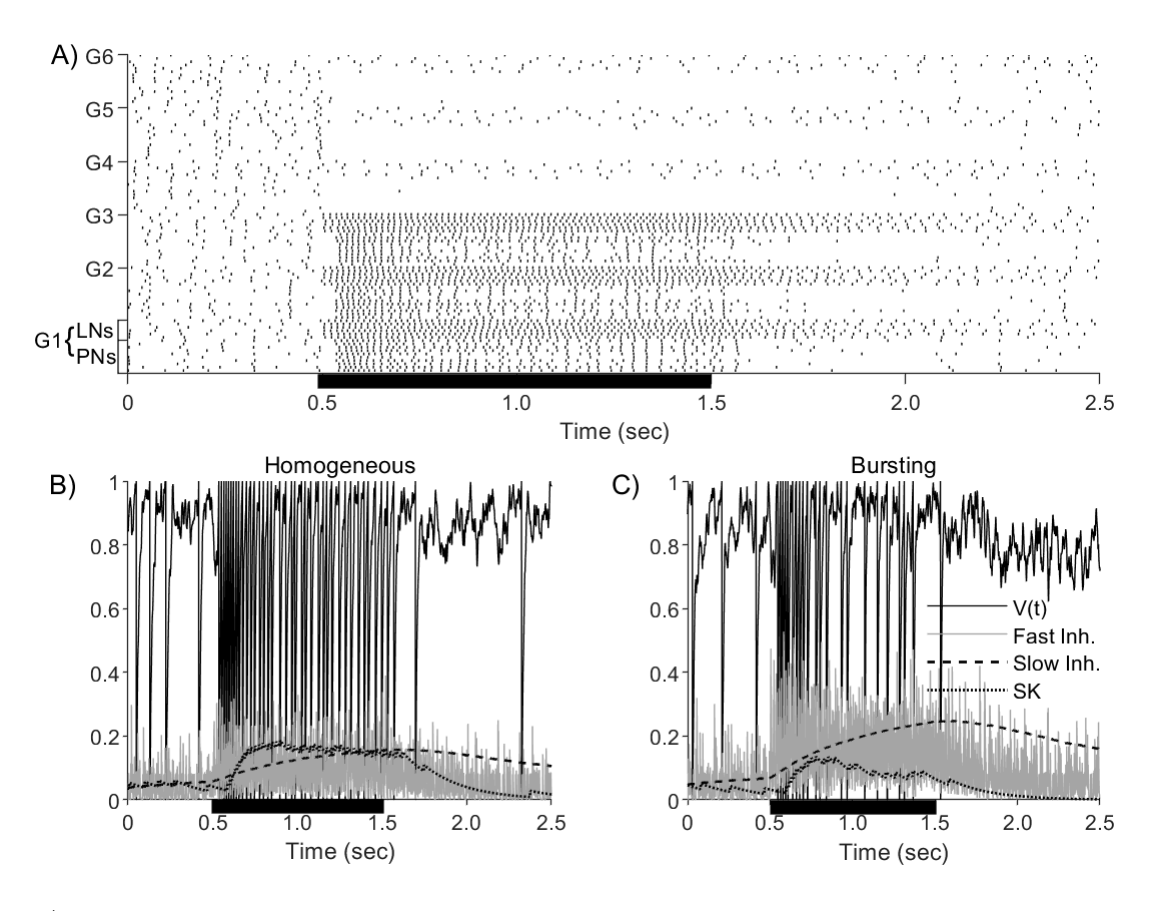


Figure 4: Figure 4. Model dynamics in response to odor stimulation alone, with no mechanosensory input. (A) Spike raster of the AL network. PNs and LNs are grouped together by glomerulus, with the bottom 10 rows in each glomerulus depicting PNs and the top 6 rows depicting LNs. A one second odor pulse (marked by the black bar on the horizontal axis) is simulated by sending stimulus current to all cells within glomeruli 1,2 and 3. (B) Plot of the membrane potential, intrinsic SK current, and incoming synaptic excitation, slow inhibition, and fast inhibition for a single PN in a stimulated glomerulus. This PN displayed continuous firing behavior. (C) Similar plot as (B), but for a neuron which displayed a more burst-like firing pattern.

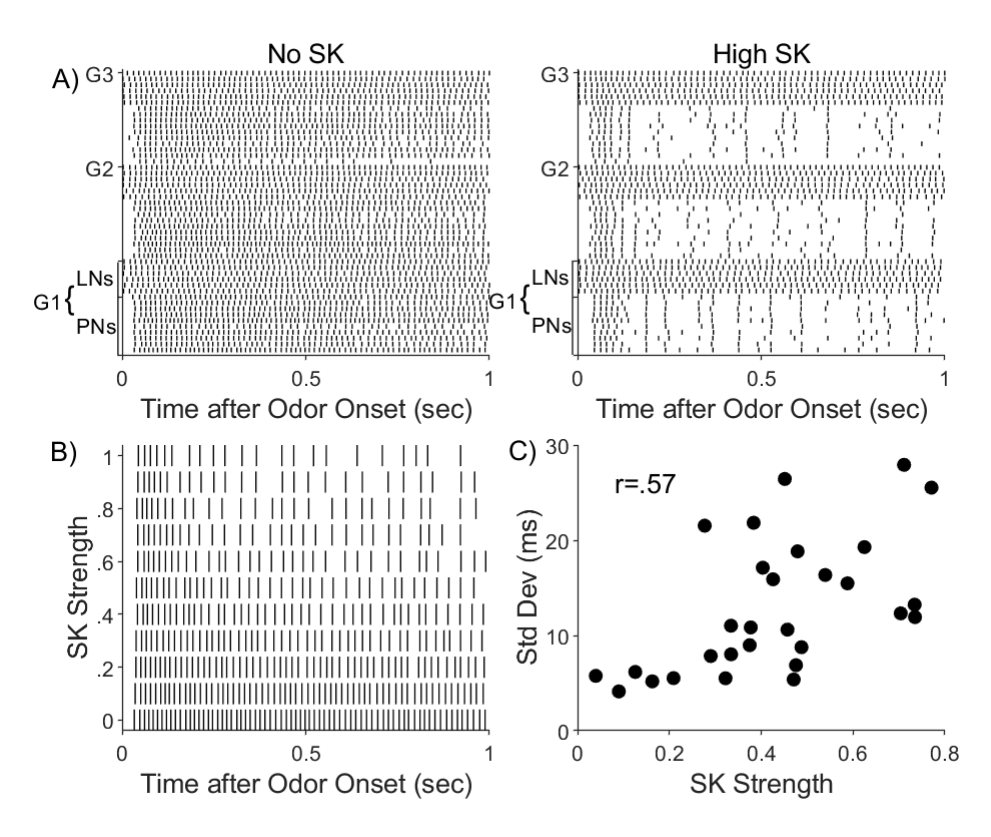


Figure 5: Figure 5. (A) Raster plot of model dynamics during a one second odor pulse (with no mechanosensory input), in the case that all PNs either have no SK currents (left) or very strong SK currents (right). Note that PNs without SK current exhibit more continuous firing, whereas PNs with high SK currents exhibit more burst-like behavior. (B) Spike rasters for a single stimulated PN in the model during a 1 second odor pulse, for varying levels of the strength of the PN's SK current. As SK strength increases, firing behavior shifts from being continuous to bursting. (C) The standard deviation of interspike interval during odor stimulation was used to quantify the burstiness of a PN. A small standard deviation represents relatively homogeneous firing, while a larger standard deviation represents fluctuations between short interspike intervals within a burst and long interspike intervals between bursts. The scatter plot shows SK strength and standard deviation in interspike interval for each PN during odor presentation (only PNs within active glomeruli are included). A positive correlation of r=0.57 reveals that SK currents indeed play a role in the emergence of heterogeneous bursting behavior.

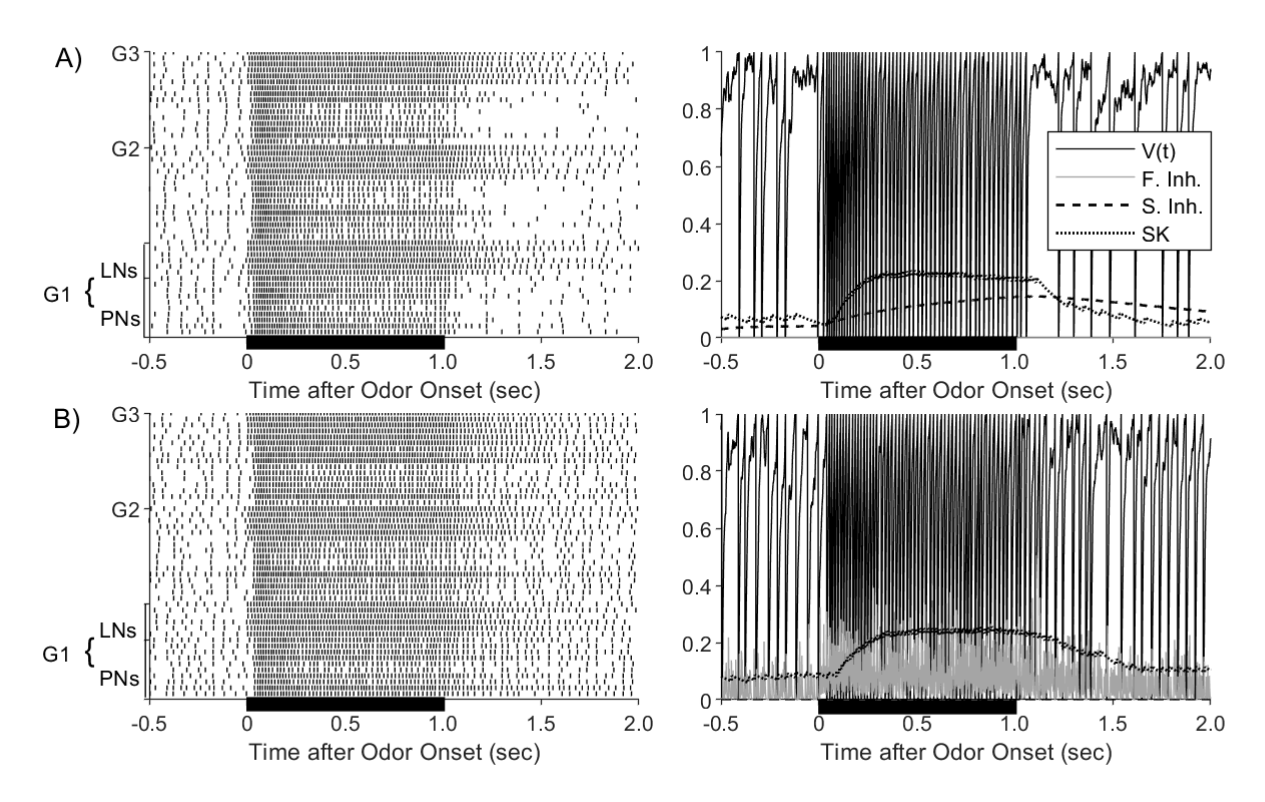


Figure 6: Figure 6. (A) Raster plot of the model AL during odor presentation with no mechanosensory input (left) and membrane potential, SK current, incoming synaptic excitation, slow inhibition, and fast inhibition for a sample PN (right); plots shown are in the case that fast inhibition is removed from the network. Note that removing fast inhibition diminishes the phase I hyperpolarization ( $I_1$ ) of PNs upon odor onset. (B) Similar plots as in (A), but with slow inhibition rather than fast inhibition removed from the network. Note that removing slow inhibition eliminates the prolonged AHP phase ( $I_2$ ) of PNs following odor offset. Black bar represents odor stimulus.

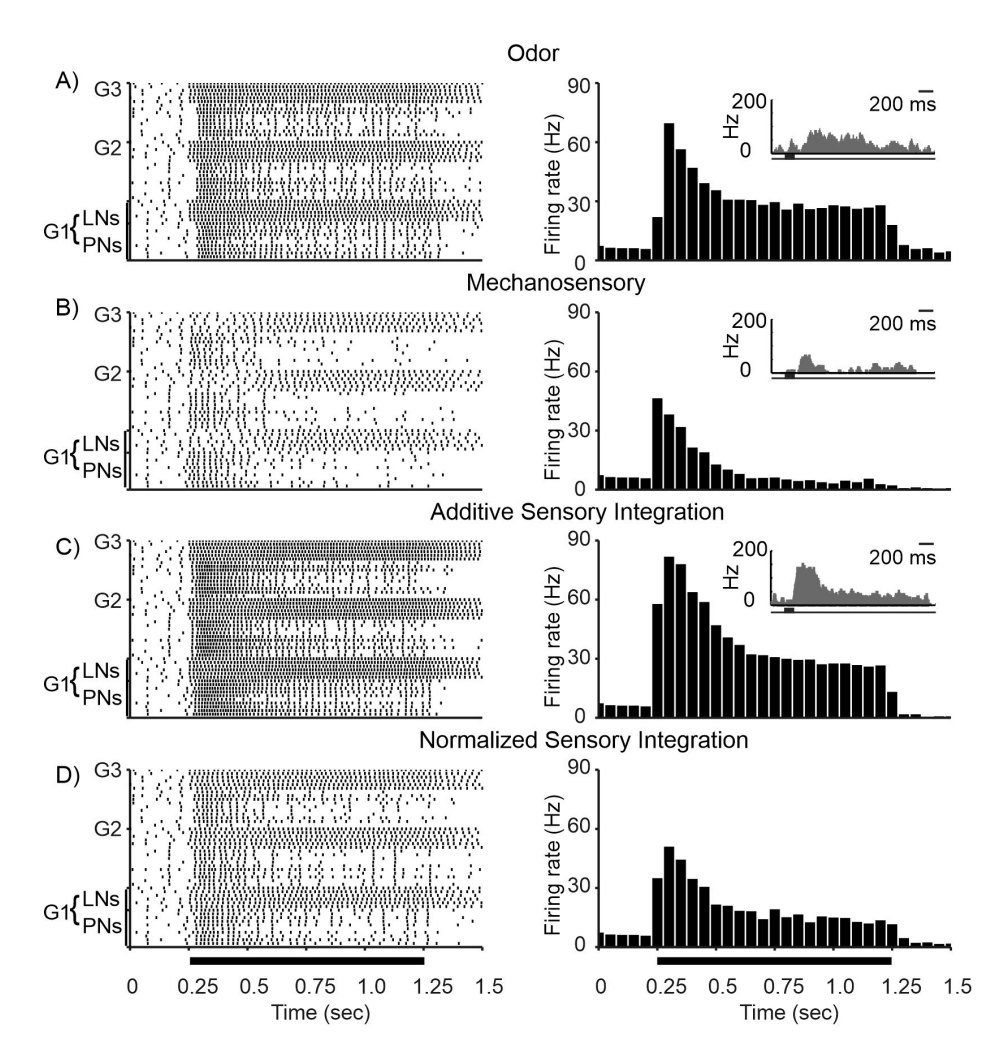


Figure 7: Figure 7. Raster plots of the first three model glomeruli (left) and firing rates of a sample PN from one of these glomeruli over 10 ms windows and averaged over 100 trials (right) for (A) odor input only, (B) mechanosensory input only, (C) additive odor and mechanosensory integration, and (D) normalized odor and mechanosensory integration. These results closely mimic the experimental results shown in figure 1, displayed in panel insets on the right for comparison. Black bar represents stimulus; different trials in the same stimulus condition correspond to different instantiations of the Poisson noise received by each neuron, with network connectivity and parameters fixed across trials.

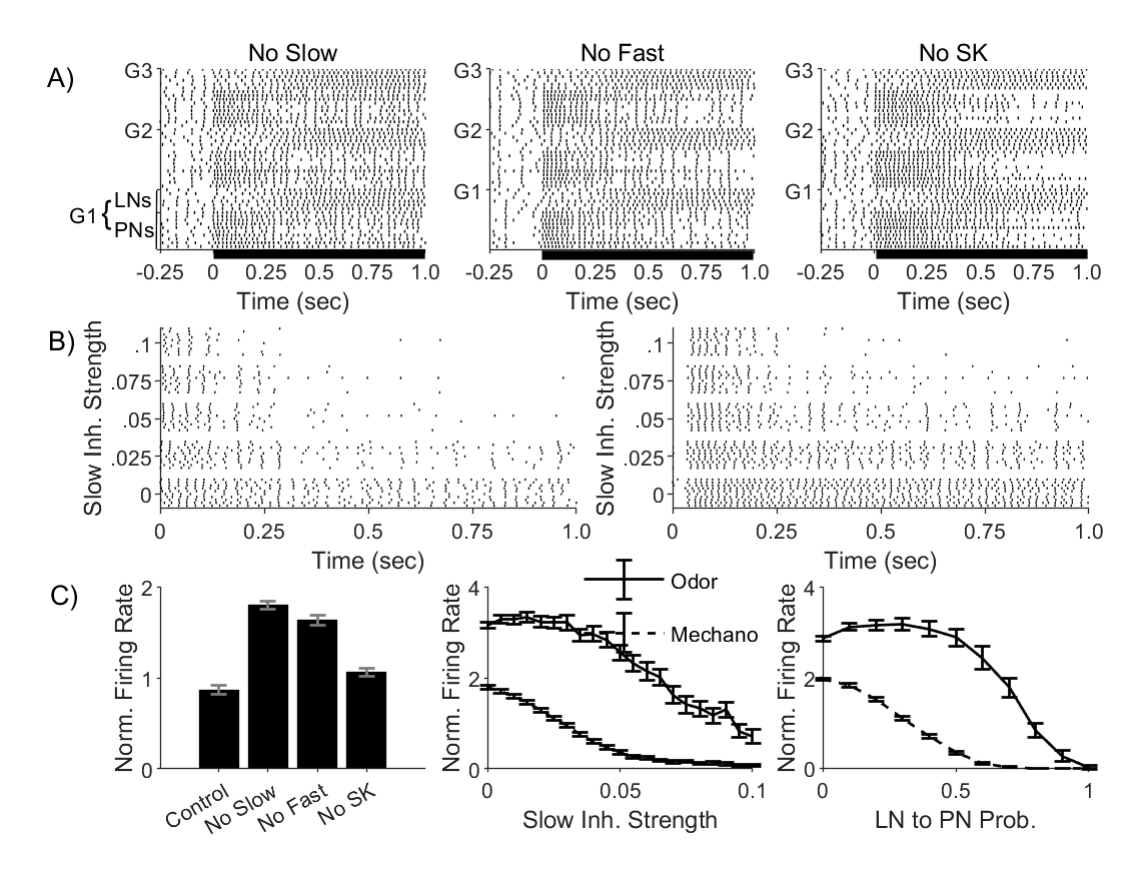


Figure 8: Figure 8. (A) Raster plots of three sample glomeruli within the model AL during AL stimulation by a 1 second pulse of mechanosensory input only (black bar), in the case where slow inhibition is removed (left), fast inhibition is removed (center), or the SK current is removed (right) from the model. Slow inhibition appears to have the largest effect in causing the transient nature of the mechanosensory response. (B) Raster plots of a sample stimulated glomerulus during AL stimulation by a 1 second pulse of mechanosensory input only (left) or odor input only (right) for varying strengths of the slow inhibitory synapses from LNs to PNs. As slow inhibitory strength increases, both mechanosensory and odor responses appear more transient, though the mechanosensory response becomes transient at lower slow inhibitory strengths than the odor response. (C) Left: Bar plot for PN firing rate, averaged over all network PNs and normalized by the background firing rate, during the last 500 ms of a 1 second pulse of mechanosensory input only. Data are shown in the case of the fully intact model (control) as well as in cases where various network components are removed. Mean and standard deviations are computed over 100 trials. Note that, without slow inhibition, there is little response suppression during the last 500 ms of the stimulus pulse. Center: PN firing rate, averaged over all network PNs and normalized by the background firing rate, during the last 500 ms of a 1 second pulse of mechanosensory input only or odor input only, as a function of the strength of slow inhibitory synapses. Mean and standard deviations are computed over 100 trials. Right: Same as in the center panel, except PN firing rate is plotted as a function of the density of LN-PN synapses. Note that during the latter half of a stimulus pulse the response to mechanosensory input alone, compared to the response to odor input alone, is suppressed at lower values of slow inhibitory strength or LN $\rightarrow$ PN connection probability.

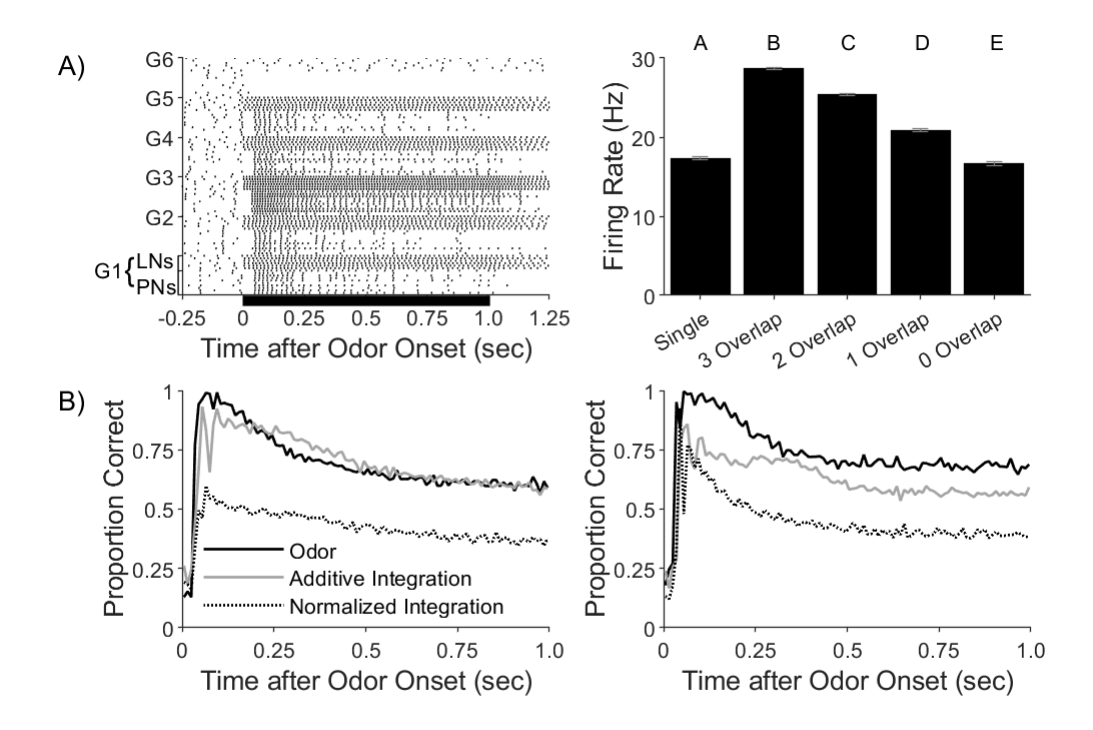


Figure 9: Figure 9. (A) Left: Raster of model AL network spikes in response to simultaneous presentation of two odors (without mechanosensory input). Odor 1 stimulated glomeruli 1, 2, and 3; odor 2 stimulated glomeruli 3, 4, and 5. Right: Bar chart of PN firing rate, averaged over the entire AL, for simultaneous presentation of two odors with various degrees of overlap in the glomeruli activated by each odor; data show means and standard deviations computed over 100 trials (differing letters above bars indicate p < 0.05 statistical significance). The less the overlap in stimulated glomeruli, the greater the suppression of PN responses, likely due to greater AL-wide activation of the LN network. (B) Left: Plots of the odor classification rate of net PN activity during a one second period of odor presentation for the odor only, additive odor and mechanosensory, and normalized odor and mechanosensory stimulus scenarios. A panel of 20 odors was employed, and the correct classification rate of net PN activity was computed in 10 ms windows using a simple linear classification scheme (see Methods for details). Right: Same plot as in the left panel, except with slow inhibition removed from the model.